

1 The effect of low solubility organic acids on the
2 hygroscopicity of sodium halide aerosols

3

4 Lorena Miñambres*, Estíbaliz Méndez, María N. Sánchez, Fernando Castaño and Francisco J.
5 Basterretxea

6

7 *Departamento de Química Física*

8 *Facultad de Ciencia y Tecnología*

9 *University of the Basque Country, UPV/EHU*

10 *Campus de Leioa*

11 *B. Sarriena, s/n*

12 *Leioa 48940 SPAIN*

13

14

15

16

17

18

19

20

21

22

23

24 *Corresponding author

25 Lorena Miñambres

26 Phone: +34 94 601 5386

27 Fax: +34 94 601 3500

28 E-mail address: lorena.minambres@ehu.es

29

30

31

32 **ABSTRACT**

33

34 In order to accurately assess the influence of fatty acids on the hygroscopic and other
35 physicochemical properties of sea salt aerosols, hexanoic, octanoic or lauric acid together with
36 sodium halide salts (NaCl, NaBr and NaI) have been chosen to be investigated in this study. The
37 hygroscopic properties of sodium halide submicrometer particles covered with organic acids have
38 been examined by Fourier-transform infrared spectroscopy in an aerosol flow cell. Covered
39 particles were generated by flowing atomized sodium halide particles (either dry or aqueous)
40 through a heated oven containing the gaseous acid. The obtained results indicate that gaseous
41 organic acids easily nucleate onto dry and aqueous sodium halide particles. On the other hand,
42 Scanning Electron Microscopy (SEM) images indicate that lauric acid coating on NaCl particles
43 makes them to aggregate in small clusters. The hygroscopic behaviour of covered sodium halide
44 particles in deliquescence mode shows different features with the exchange of the halide ion:
45 whereas the organic surfactant has little effect in NaBr particles, NaCl and NaI covered particles
46 experience appreciable shifts in their deliquescence relative humidities, with different trends
47 observed for each of the acids studied. In efflorescence mode, the overall effect of the organic
48 covering is to retard the loss of water in the particles. It has been observed that the presence of
49 gaseous water in heterogeneously nucleated particles tends to displace the cover of hexanoic acid to
50 energetically stabilize the system.

51

52

53 **Keywords:** marine aerosol, fatty acids, heterogeneous nucleation, hygroscopicity.

54

55 1. INTRODUCTION

56

57 Marine aerosol is one of the most abundant types of natural particulate matter in the Earth's
58 troposphere. Sea salt particles play an active role in the Earth's radiative balance, influence mass
59 transfer of gaseous compounds and cloud-precipitation mechanisms, contribute to the formation of
60 cloud condensation nuclei and have highly reactive surfaces that take part in heterogeneous and
61 multiphase chemical reactions (Andreae and Rosenfeld 2008; Carslaw et al 2010; D O'Dowd and
62 De Leeuw 2007; Finlayson-Pitts 2003; Lewis and Schwartz 2004; Quinn and Bates 2011; Rossi
63 2003). They also can uptake significant amounts of water, exhibiting deliquescence and
64 efflorescence properties under atmospheric conditions (Freney et al 2009; Martin 2000; Metzger
65 and Lelieveld 2007; Mikhailov et al 2013; Wise et al 2012), that can change the particles' phase and
66 size, together with other interrelated physico-chemical properties: for example, water uptake
67 increases particle size, thus favouring their sedimentation. In parallel, bigger particles increase the
68 scattering of solar visible light, thus influencing atmospheric radiative transfer and visibility. The
69 presence of water in atmospheric particles can also change the adsorption of trace gases and their
70 chemical reactivity (e.g., sulfate chemistry proceeds by adsorption of gaseous SO₂ on aqueous
71 particles, followed by oxidation to sulfate; this pathway is absent in crystalline particles).

72 Marine aerosol is generated either by the mechanical action of the ocean surface (primary
73 sea-salt aerosol), or by gas-to-particle conversion processes (secondary aerosol) mainly in the form
74 of nonsea-salt sulphate and organic species (O'Dowd et al 1997). Sodium chloride is the principal
75 component of sea salt: typical sea water composition has 1.05×10^4 mg/L of Na⁺ and 1.9×10^4 mg/L
76 of Cl⁻ (Lide 1994). Bromide ions are a minor component of seawater, and hence of sea salt particles,
77 with a molar ratio of bromide to chloride of 1:650 (Lide 1994). Despite such a small contribution to
78 the composition of sea salt particles, bromine plays a comparatively large role in tropospheric sea
79 salt chemistry. The most important is the drop of surface-level ozone concentrations in the Arctic at
80 polar sunrise. This is due to the tendency of Br⁻ to segregate to the salt surface in the presence of
81 water, substantially increasing Br/Cl surface molar ratios, and to the fact that bromide ions exhibit a
82 higher surface reactivity than chloride (Baker 2005; Ghosal et al 2008; Zangmeister et al 2001). Sea
83 salt particles have been shown to be the source of BrO, which is involved in catalytic cycles that
84 destroy ozone (Finlayson-Pitts 2009; Frinak and Abbatt 2006; Hunt et al 2004; Read et al 2008;
85 Von Glasow 2008). Although the concentrations of I⁻ present in seawater are much smaller than
86 those of bromine and chlorine (the molar ratio of I⁻ to Cl⁻ in seawater is $\sim 1:10^6$), there is evidence
87 that iodine in the marine boundary layer has an influence on ozone destruction, the oxidizing

88 capacity of the troposphere, denoxification, and particle formation (Carpenter 2003; Saiz-Lopez et
89 al 2008). A similar role to BrO is played by IO, although its source is believed to come from marine
90 algae (Read et al 2008). Recently advances have been made in quantifying the link between
91 seawater chemical processes, and the production, size, and chemical composition of sea spray
92 aerosol particles by simultaneous measurements of seawater, particle size distributions, and size-
93 resolved single particle chemical composition in a laboratory setting reproducing the chemical
94 complexity of sea spray aerosol, including natural seawater, breaking waves and controlled
95 phytoplankton and heterotrophic bacteria concentrations (Ault et al 2013; Prather et al 2013). It has
96 been shown that the mixing state of sea aerosol is sensitive to the presence of heterotrophic bacteria,
97 that transform dissolved organic matter.

98 Organic compounds are present in marine salt aerosol in variable proportions that may
99 represent a large fraction of the aerosol dry mass (Cavalli et al 2004; Gantt and Meskhidze 2013;
100 Middlebrook et al 1998). The presence of significant concentrations of organic matter in marine
101 aerosol was detected in earlier studies (Kleefeld et al 2002; Middlebrook et al 1998; Putaud et al
102 2000). Measures over the North Atlantic Ocean have revealed that the organic fraction contributes
103 up to 63% to the submicrometer aerosol mass, of which about 45% is water-insoluble and 18%
104 water-soluble (O'Dowd et al 2004). 37% hydrocarbon and 63% oxygenated hydrocarbon speciation
105 was observed for the organic mass indicating that at least 37% of the organic mass is produced via
106 primary sea-spray (Ovadnevaite et al 2011a). It was found that predominantly organic particles
107 contribute between 25 and 30% to general background marine number concentration, 35% for open
108 ocean nucleation cases, and 60% for anthropogenically influenced cases (Bialek et al 2012). The
109 organic fraction of marine aerosol can be highly enriched due to oceanic biological activity (Ault et
110 al 2013; Gantt and Meskhidze 2013; O'Dowd et al 2002; Ovadnevaite et al 2011a; Rinaldi et al
111 2010). Much of the organic fraction corresponds to water insoluble fatty acids present as surface
112 films on particles (Donaldson and Vaida 2006; Mochida et al 2002; Tervahattu et al 2002), but also
113 as organic carbon more homogeneously mixed with cations and anions (Ault et al 2013).

114 Moreover, fine mode marine organic aerosol can have a size distribution independent from
115 that of sea-salt, while coarse mode aerosols are more likely to be internally mixed with sea-salt
116 (Gantt and Meskhidze 2013). Primary marine aerosols mixed with a surfactant can be generated by
117 wind action on the sea surface, which is covered by a low solubility organic layer (Donaldson and
118 Vaida 2006). Alternatively, heterogeneously nucleated particles can form when low vapor pressure
119 organic vapors condense on pre-existing aerosol particles, forming a surface coating, that can be
120 evenly or unevenly distributed. It has been proposed that the organic compounds arrange in a
121 hydrophobic organic monolayer that encapsulates an aqueous particle, forming an “inverted

122 micelle” structure (Ellison et al 1999). This model shows agreement with recent molecular dynamic
123 simulation results (Chakraborty and Zachariah 2008). Other models predict that certain fatty acids
124 form pockets of micelles within the aerosol, modifying the surface tension of the particle and
125 therefore changing the water uptake properties of atmospheric aerosols (Tabazadeh 2005), and that
126 core-shell structures are not always the most stable (Kwamena et al 2010), again affecting the
127 particle water uptake properties and optical properties.

128 The presence of an organic film at the surface of a particle may affect its physical and
129 chemical properties in a number of ways. The film may act as a barrier to transport across the
130 interface, inhibiting uptake of atmospheric gases or reactions between gas phase reactants and
131 particle surface, such as the heterogeneous reaction $\text{NaCl(s)} + 2\text{NO}_2(\text{g}) \rightarrow \text{ClNO}(\text{g}) + \text{NaNO}_3(\text{s})$
132 (Donaldson and Vaida 2006; Finlayson-Pitts 2003). In particular, the surface film can affect the
133 process of cloud condensation nuclei formation and aerosol growth to climatically relevant sizes
134 (Andrews and Larson 1993; Chuang 2003). Organic compounds can also change the amount of
135 light scattered by inorganic particles (Dall'Osto et al 2010; Fierz-Schmidhauser et al 2010; Vaishya
136 et al 2013). Marine primary organic aerosol (POA) can cause large local increases in the cloud
137 condensation nuclei concentration by 15% to more than 100% (O'Dowd et al 2004; Ovadnevaite et
138 al 2011b), and the ambient mass concentration and organic mass fraction of sea-spray aerosol are
139 related to surface ocean biological activity. Despite considerable work has been carried out in the
140 last years, there is still much uncertainty about fundamental properties of marine aerosol particles,
141 such as chemical composition, mixing state, hygroscopicity, cloud droplet activation, formation,
142 aging and removal mechanisms (Gantt and Meskhidze 2013; IPCC 2013). Several laboratory
143 studies about the effect of organic surfactants, such as palmitic and oleic acids, on NaCl,
144 ammonium sulfate or mineral dust aerosol particles as a function of relative humidity have been
145 reported employing a variety of experimental techniques, such as electrodynamic balance, infrared
146 spectroscopy, electrical mobility, optical tweezers, cavity ring-down spectroscopy or nonlinear
147 spectroscopy (Cwiertny et al 2008; Davies et al 2013; Dennis-Smith et al 2012; Ebben et al 2013;
148 Garland et al 2005; Hansson et al 1998; Najera and Horn 2009; Robinson et al 2013; Rossi 2003;
149 Rubasinghege et al 2013). The general conclusions are that hygroscopic growth, deliquescence
150 relative humidity (DRH) and efflorescence of the particles at efflorescence relative humidity (ERH)
151 may be affected by several factors, such as coating thickness or structural arrangement of the
152 organic film. Special effort has been carried out to study the morphology and phase partitioning of
153 aerosol particles consisting of hydrophobic and hydrophilic phases (Ciobanu et al 2009; Kwamena
154 et al 2010; Reid et al 2011; Veghte et al 2013). On the other hand, molecular dynamics calculations
155 are becoming a commonplace theoretical approach in atmospheric aerosol modeling that includes

156 sea salt particles mixed with organic molecules (Ma et al 2011; Sun et al 2012; Sun et al 2013;
157 Takahama and Russell 2011).

158 As a whole, laboratory studies on inorganic particles coated with surfactant organics have
159 mainly focused on a few organic molecules, and most of them have been carried out with
160 ammonium sulfate or sodium chloride. Very few studies of hygroscopic behavior have been carried
161 out on particles containing bromide or iodide. Furthermore, sodium chloride, bromide and iodide
162 particles exhibit very different hygroscopic properties and interact differently with water soluble
163 dicarboxylic acids such as succinic acid (Minambres et al 2011). It has been reported that rates of
164 gaseous iodine emissions during the heterogeneous reaction of O₃ with interfacial iodide are
165 enhanced several-fold by the presence of alkanolic acids on water, such as octanoic and hexanoic
166 acid (Hayase et al 2011). In the present work we study the hygroscopic properties of NaX (X=Cl,
167 Br, I) sodium halide salts coated with either one of three different surfactant carboxylic acid
168 molecules by Fourier-transform infrared extinction spectroscopy in an aerosol flow tube, aided by
169 particle sizing methods. The examined acids, all contain one carboxylic group at the end of the
170 molecule, are hexanoic (CH₃(CH₂)₄COOH), octanoic (CH₃(CH₂)₆COOH) and dodecanoic or lauric
171 acid (CH₃(CH₂)₁₀COOH), hereafter shortened as HA, OA and LA, respectively. These acids belong
172 to the family of alkanolic acids, that make a significant proportion of the organic compounds emitted
173 from several sources to the atmosphere, such as seed oil and meat cooking procedures or emission
174 by plants. The substances emitted in coastal areas can condense onto preexisting marine aerosol and
175 modify their properties. HA, OA and LA have been observed in the atmosphere of remote marine
176 and continental locations (Duce et al 1983; Gill et al 1983; Limbeck and Puxbaum 1999; Samy et al
177 2010; Schauer et al 1999; Schauer et al 2002; Yassaa et al 2001). OA and LA exist as liquid and
178 solid, respectively, at typical tropospheric temperatures and pressures. HA has higher vapor
179 pressure than the atmospherically more abundant long chain acids that may contribute more
180 substantially to vapor phase processes. HA, OA and LA have water solubilities of 9.9, 0.68 and
181 0.058 g/L at 20°C, respectively (see Table 1), and have been selected as they are expected to
182 influence the hygroscopic behaviour of sea-salt particles differently in view of their water
183 solubilities: HA has intermediate solubility between highly soluble and highly insoluble organic
184 acids, whereas LA, on the other end, can represent highly insoluble fatty acids, OA lying in-
185 between. Due to their overall low water solubility, pure fatty acids are not expected to present
186 significant intrinsic hygroscopic properties.

187 A few studies have been presented describing the effects of octanoic and lauric acids on the
188 hygroscopicity of NaCl (Hämeri et al 1992; Hansson et al 1998; Wagner et al 1996). The results
189 indicate that formation of organic surfactant layers tend to slow NaCl deliquescence rate and to

190 slightly lower its DRH. This may affect particle size and phase, changing the amount of scattered
191 solar radiation and also the adsorption behavior of trace gases onto particles. Molecular dynamics
192 simulations of water vapor molecules impinging on a slab of water coated by octanoic acid film
193 showed that the mass accommodation coefficient decreased with the degree of surface coverage of
194 the hydrocarbon backbones (Takahama and Russell 2011).

195

196

197 **2. MATERIALS AND METHODS**

198

199 Infrared spectroscopy is a well-known sensitive technique and has been applied to the study
200 of organic/inorganic aerosol systems (Garland et al 2005; Najera and Horn 2009). It can yield
201 aerosol composition, water content, and particle phase. Variations in the wavenumbers and widths
202 of spectral bands (precisely their FWHM: full width at half maximum) can also reveal information
203 about molecular interactions in mixed systems and the formation of new species. Infrared spectra
204 have been combined with electron scanning microscopy (SEM) of particles, a technique that has
205 been demonstrated to be useful to study the chemistry of isolated, individual particles of
206 atmospheric relevance (Krueger et al 2003; Veghte et al 2013).

207 The configuration of the experimental setup used in this work is based on a system described
208 previously (Minambres et al 2010), that has been modified for the present study. The main elements
209 are depicted in Figure 1. Submicrometric particles are formed by injecting a 0.01 kg/L aqueous
210 solution of sodium halide salts (NaCl, NaBr and NaI, $\geq 98\%$) in a commercial atomizer (TSI 3076).
211 Their relative humidity (RH) can be controlled (from 0 to around 95%) by combining two serially
212 connected diffusion driers and a flow of N_2 with a controlled amount of water vapor. RH is
213 measured with a digital thermohygrometer (Vaisala Humicap HMT 337) placed at the exit of the
214 aerosol flow cell (see Figure 1). The measurement error is 1% RH in the 0-90% RH range, and
215 1.7% outside it. Hygrometer absolute RH values were periodically checked against a calibration
216 curve obtained by recording the integrated infrared absorption of water vapor (measured from 2166
217 to 1188 cm^{-1} in the H_2O bending ν_2 fundamental band) flowing through the aerosol cell at selected
218 RH values (measured with the hygrometer). Measurements are carried out after the RH of the
219 aerosol flow reaches a constant value with fluctuations within the RH measurement error. The
220 inorganic particles are coated by passing the aerosol flow (1.8 L/min) through a heated cell that
221 contains a sample of either hexanoic (99%), octanoic ($\geq 98\%$), or lauric acid ($\geq 98\%$). Table 1

222 summarizes the most relevant physical properties of these acids.

223 The heating cell consists of an horizontally-set cylindrical borosilicate glass tube 30 cm long
224 having 3 cm internal diameter, that has two smaller glass tubes (30 and 20 cm long, 1 cm internal
225 diameter) coaxially attached at its ends. Acid sample (either liquid or solid) is placed uniformly
226 along the central tube. The whole cell is thermally isolated by wrapping it with alumino-silicate
227 refractory ceramic fiber. To allow for sufficient vaporization of the acid, the central tube and exit
228 arm of the cell are heated up to 100°C by means of flexible resistors coiled around them. The
229 temperatures at both cell locations (T_1 refers to the central part, T_2 to the exit arm, see Figure 1) are
230 controlled by placing two K-type thermocouples at the cell outer walls. To form heterogeneously
231 nucleated particles, T_1 was varied from 75 to 100°C and T_2 from 60 to 90°C. Higher temperature
232 indicates higher concentration in the gas phase leading to enhanced condensation and larger
233 particles and therefore thicker coating. The temperature measurement errors are estimated to be in
234 the 4-7°C range (the higher value corresponds to the highest temperature). A prominent baseline
235 shift was observed in all cases, in agreement with particle formation. This shift increases with T_1
236 and T_2 , indicating bigger particles. Purely homogeneously nucleated particles were formed by
237 passing a flow of gaseous nitrogen through the heated oven at $T_1=80-100^\circ\text{C}$ and $T_2=60-90^\circ\text{C}$
238 containing the carboxylic acid. This coating method can get a reproducible amount of fatty acid on
239 particles in a fast and convenient way, and has been used by other authors in laboratory experiments
240 (RW.ERROR - Unable to find reference:18; Abbatt et al 2005; Garland et al 2008; Rouviere and
241 Ammann 2010; Stemmler et al 2008) Although in the troposphere the whole process of
242 heterogeneous nucleation of organic vapors takes place at overall lower temperatures, in our
243 experiment the heated organic vapor gets in contact with the nitrogen gas flow at ambient
244 temperature that effectively cools the vapor by rapid heat exchange (the number density of nitrogen
245 molecules in the gas flow is much higher than the number density of organic vapor molecules in the
246 tube). Eventually, cooled gas-phase organic molecules heterogeneously nucleate on salt particles in
247 the nitrogen gas flow. In that way, the way to generate heterogeneously nucleated particles can be
248 assumed to follow the same physical process than in the atmosphere, although the temperatures can
249 vary over a broad range.

250 The final aerosol flux was directed simultaneously to a condensation particle counter (CPC,
251 either TSI 3781 or MSP 1040XP models, inlet flow 0.6 L/min), an aerodynamic particle
252 spectrometer (APS, TSI 3321, inlet flow 1.0 L/min) and a Fourier-transform infrared spectrometer
253 (Nicolet Magna 860), to obtain particle number, size distribution and their infrared extinction
254 spectra, respectively. Infrared extinction spectra are recorded in the 650-4000 cm^{-1} range and 4 cm^{-1}
255 resolution. Infrared radiation from a collimated source (ORIEL 6580) travels lengthways a 1 m

256 long, 50 mm diameter Pyrex absorption cell at ambient temperature with ZnSe windows. The
257 outgoing radiation is directed to the infrared spectrometer (Figure 1), where the infrared beam is
258 divided into two. Both beams take slightly different path lengths, and recombine to construct an
259 interferogram. The recombined intensity is recorded as the path length difference is changed. By
260 applying the Fourier transform technique, the variation of the intensity with wavenumber is
261 retrieved. The optical path is sealed and flushed by a current of dry air to reduce interference from
262 ambient water and carbon dioxide. Background spectra are recorded after pumping out the aerosol
263 cell. Sample spectra are averaged by collecting typically 32 scans. To complete analytical on-line
264 methodology, particle shape and size of both pure and mixed particles were determined off-line
265 using a JEOL JSM-7000F scanning electron microscope (SEM), equipped with a Schottky field
266 emission gun (FEG) and an Oxford Inca Pentafet X3 energy dispersive X-ray analyzer (EDX). The
267 EDX microanalysis was performed using an accelerating voltage of 20 kV and a current intensity of
268 10^{-10} A with a working distance of 10 mm. The aerosol of interest was collected at the exit of the
269 extinction flow cell onto a glass slide, and particles were coated with an Au layer (20 nm) deposited
270 by evaporation using a Quorum Q150T Sputter Coater to provide electrical conductivity.

271 Particle size distribution in the 0.5-20 μm is retrieved by an aerodynamic particle
272 spectrometer (TSI 3321), that give a tail in the 0.5-3.5 μm range. Information about the size
273 distribution of pure salt particles in the 0-0.5 μm range was obtained by processing the SEM images
274 with the help of the ImageJ software [rsbweb.nih.gov/ij/]. The obtained distribution fitted
275 satisfactorily to a lognormal distribution with a count median diameter of 46 nm and $\sigma = 2.0$.
276 Particles appear mostly isolated without a tendency to aggregate. Representative examples of
277 number size distributions of pure NaCl particles and also covered with hexanoic acid are presented
278 in Figure 2.

279 The amounts of liquid water and a given organic acid in the particles can be calculated on
280 average from measured absorbances in their infrared spectra. The number of molecules N_i of a
281 given species i per unit volume of aerosol sample is related with the integrated band absorbance of
282 that species via the Beer-Lambert law (Weis and Ewing 1996): $\bar{A}_i = \bar{\sigma}_i N_i z / 2.303 \times 10^2$, where \bar{A}_i is
283 the integrated absorbance of a given band (cm^{-1}), $\bar{\sigma}_i$ the integrated absorption cross section per
284 molecule (m molecule^{-1}) of that band, and z is the optical path length of the aerosol flow cell (m).
285 The $\bar{\sigma}_i$ value can be taken from the literature or measured independently. The concentration of Na^+
286 and X^- ions cannot be quantified by this method, as monoatomic ions do not present vibrational
287 spectra.

288

289 3. RESULTS AND DISCUSSION

290

291 3.1. Infrared spectra of pure carboxylic acids

292

293 The infrared absorption spectra of bulk HA, OA and LA recorded at ambient temperature
294 are presented in Figure 3. The spectra of HA and OA were recorded in an infrared cell for liquids,
295 whereas for LA one drop of the sample dissolved in ethanol was deposited on a BaF₂ window until
296 solvent evaporation, after which the absorption spectrum of the film was recorded. The main
297 absorption bands are common to all three acids, with small differences in band position and
298 intensity.

299 The sharp carbonyl stretching band can be seen near 1710 cm⁻¹, the broad band in the 2500-
300 3500 cm⁻¹ range has been assigned to associated COO-H stretchings (broadened by intermolecular
301 association by hydrogen bonding), whereas the group of three peaks in the 2800-3000 cm⁻¹ range,
302 exhibiting a different resolvable structure for the different acids, has been assigned to -C-H
303 stretchings. A more complex band system appears in the 800-1500 cm⁻¹, specific of each acid. On
304 the other hand, the gas phase infrared spectra of the three acids (NIST Chemistry Webbook:
305 <http://webbook.nist.gov/chemistry>, not shown in Figure 3) show several differences with the bulk
306 phase spectrum: the intense C=O band locates in the 1780-1790 cm⁻¹, whereas a narrow band
307 appears near 3580 cm⁻¹ (COO-H free stretch), absent in the condensed phase. Overlapped bands
308 appearing in the 2800-3000 cm⁻¹ range are coincident with peak positions in bulk phase spectra.
309 Finally, a number of bands are present in the 800-1600 cm⁻¹ region, several of which can be
310 distinguished from condensed phase spectra.

311 Figure 3 also shows the extinction spectra of pure, homogeneously nucleated particles.
312 Bands belonging to each acid were detected in all cases, their absorption intensity growing with
313 increasing T₁ and T₂. CPC measurements confirmed the presence of particles that were assumed to
314 be composed of pure carboxylic acids. For HA the obtained spectra is mostly coincident with the
315 gas phase spectrum. A weak band located at near 1730 cm⁻¹ has been assigned to the C=O stretch
316 originating from small particles of liquid HA due to homogeneous nucleation. This band is 21 cm⁻¹
317 displaced to higher wavenumbers with respect to bulk liquid HA, possibly due to surface effects in
318 small particles: due to the interactions between surface molecules and the surrounding medium, the
319 surface region has different structural properties (and thus spectroscopic features) than the core of
320 the particles (Firanescu et al 2006). This hypothesis is supported by the spectrum of liquid HA

321 adsorbed at the air/water interface by vibrational sum-frequency spectroscopy (Soule et al 2007),
322 that locates the C=O band in the 1726-1730 cm^{-1} range, depending on the polarization conditions.
323 For OA, the C=O band was peaked at near 1700 cm^{-1} , but broader than the one corresponding to
324 condensed phase. Also an overlapping band system in the 1540-1650 cm^{-1} range was observed. No
325 lines of gaseous OA were detected. For LA, no gas band features were present, in accordance with
326 its low vapor pressure. Further evidence of the presence of particles is given by the baseline
327 increase to higher wavenumbers (Figure 3), which is indicative of particle scattering (Hinds 1998).
328 This effect is more pronounced as T_2 is increased. A broad band in the 3100-3500 cm^{-1} range is
329 observed for homogeneously nucleated hexanoic and octanoic acid that is absent in the bulk
330 spectrum. This feature may arise from the presence of small amounts of liquid water outgassed from
331 the acid that become trapped into the particles (Safar et al 1994).

332 The most notable differences in band wavenumber and bandwidth for the three acids are
333 observed for the C=O stretching band, and are summarised in Table 2. These differences can be
334 significant, as they can be related to surface effects that can give information about the particles.
335 Carbonyl bandwidth in the bulk acids is in the 20-29 cm^{-1} range, and increases with molecular mass.
336 These values change in homogeneously nucleated organic particles, either increasing (HA and OA)
337 or decreasing (LA). Relative variations in its magnitude are in the 25-75% range.

338

339

340 **3.2. Infrared extinction spectra of heterogeneously nucleated NaX particles with carboxylic** 341 **acids**

342

343 Representative infrared extinction spectra of heterogeneously nucleated sodium halide
344 particles are shown in Figure 3. The band intensities of heterogeneous nucleation spectra are much
345 higher than those of homogeneous nucleation (e.g., 4:1 for NaCl/OA at $T_1=90^\circ\text{C}$, $T_2=80^\circ\text{C}$). For
346 NaX/HA particles, bands caused both by gaseous and condensed phase HA were observed. The
347 latter increase in intensity with T_1 and T_2 , whereas the former remain constant. For NaX covered
348 with OA or LA, practically all infrared bands originate from condensed phase, gas phase OA bands
349 being very weak or absent. The observed carbonyl absorption band wavenumber and bandwidth for
350 the various acids are collected in Table 2. The changes in these magnitudes with respect to their
351 bulk phase values are indicative of organic molecule/inorganic ion interactions, and can be used to
352 address the effect of the ionic salt environment near the organic acid molecules. For all acids the

353 C=O stretch wavenumber of the acid coating on NaX varies with the salt and is between the
354 wavenumber of the corresponding bulk acid and that of the homogeneously nucleated acid particles
355 (Table 2). In all cases, bulk wavenumber of C=O is around 70 cm^{-1} lower than in the gas phase,
356 bulk LA showing the lowest wavenumber (1700 cm^{-1}). On the other hand, the bandwidths of the
357 C=O stretch originating from heterogeneously nucleated particles depend on the nature of the salt,
358 the organic acid and the degree of covering: for HA-covered particles, the full width half-maximum
359 (FWHM) can reach 40 cm^{-1} , doubling the bulk HA value, whereas for LA-coated particles it is
360 smaller than the bulk acid bandwidth. The relationship of these results with the hygroscopic
361 properties will be discussed later.

362

363

364 **3.3. Morphology of pure and mixed particles**

365

366 SEM images of pure NaCl and LA particles, and of NaCl particles after covering them with
367 LA, were recorded and are presented in Figure 4. This technique was not well suited to study
368 particles that included OA or HA due to their high vapor pressure at room temperature that hinders
369 their manipulation in the SEM vacuum chamber. Images of pure NaCl particles show particles of
370 cubic form as expected but with their edges somewhat rounded, as a result of a short exposure of
371 deposited particles to ambient air before being coated with the gold layer. As NaCl is very
372 hygroscopic, they have uptaken a small amount of gaseous water enough to change their original
373 morphology (see Figure 4a).

374 Images of LA particles (Figure 4b) show a much smaller number of particles that tend to
375 form big aggregates, typically of $1\text{-}2\text{ }\mu\text{m}$ length. This is in accordance with previous studies
376 (Gadermann et al 2008). The particles are amorphous and elongated. Images of NaCl particles
377 deposited jointly with LA (after heterogeneous nucleation, see Figure 4c) show a small number of
378 particles, much fewer than in the case of pure NaCl, although the initial amount of NaCl aerosol
379 was identical in both cases (this may be due to the low affinity of the mixture with the supporting
380 material or to higher tube losses). Most particles present cubic form, and tend to appear as
381 aggregates. Although pure LA particles can be observed, they are very scarce. A thin layer covering
382 the NaCl particles can be observed, smaller NaCl particles appearing usually immersed in a

383 surfactant drop. Thus it can be said that a thin layer of lauric acid is deposited on NaCl particles,
384 acting as glue that tends to link individual NaCl particles.

385

386

387 **3.4. Deliquescence and efflorescence of heterogeneously nucleated NaX particles with HA, OA** 388 **and LA**

389

390 *3.4.1. Infrared spectra of particles at various RHs*

391 To examine the deliquescence behavior, dry NaX particles coated with each of the
392 carboxylic acids were mixed with a flow of gaseous water at different RHs. As a representative
393 example, Figure 5 shows three spectra of NaBr particles covered with OA at various RHs. The
394 presence of liquid water can be detected and quantified by the broad band centered at near 3400 cm⁻¹
395 ¹. For all cases, no infrared absorption bands arising from aqueous dissolved acids were detected, so
396 in all the subsequent discussion all the organic acids are assumed to be undissolved in liquid water.

397

398 In all cases we paid special attention to the C=O stretching band of the acids near 1700 cm⁻¹,
399 and we analyzed it as a function of RH, organic acid and halide anion measured. In OA/NaX and
400 LA/NaX particles the carbonyl band absorption intensity of condensed phase acid keeps constant
401 with RH. For NaX/HA particles, on the contrary, the band intensities of liquid HA decrease as RH
402 increases, although the intensities of gaseous HA remain unchanged. As an example, the spectra in
403 Figure 6 show the intensity variation of the carbonyl band near 1700 cm⁻¹ as RH is varied for liquid
404 and gaseous HA in NaBr particles in deliquescence and efflorescence modes. It can be seen that,
405 while the C=O band intensity of gaseous HA keeps roughly constant with RH, the band intensity for
406 condensed HA lowers at higher RH in deliquescence mode. The largest decrease was observed in
407 NaBr, and the smallest in NaI (not shown). In all salts, the particles retained liquid HA at RHs
408 higher than their DRH. On the other hand, the spectrum baseline in Figure 6 deliquescence spectra
409 also decreases at high wavenumber as RH increases (due to decrease of particle scattering),
410 indicating a thinner coating of the particles.

411 The efflorescence behavior of coated aqueous NaX particles was investigated by passing
412 NaX aqueous particles along the heated oven containing the carboxylic acid vapor. For all the

413 systems at RH near saturation, the spectra show bands of condensed phase organic acid. The
414 intensity of these bands keeps roughly constant with RH in OA and LA, but liquid HA band
415 intensities decrease notably as RH is reduced (a factor in the range 3-7 from RH≈100% to 27%,
416 depending on the salt). Figure 6 shows the case for NaBr/HA. Also the scattering signal is
417 decreased with RH, indicating that particles get smaller.

418

419 3.4.2. *Deliquescence and efflorescence curves*

420 Deliquescence and efflorescence curves were recorded by measuring the integrated
421 absorbance of liquid water in the particles in the 3400-3600 cm^{-1} range and plotting the values
422 versus RH. This interval was selected as it is mostly free of interference with nearby absorption
423 spectral features. The scattering component of the liquid water extinction spectrum was removed by
424 subtracting the sloping baseline present at high wavenumbers to obtain integrated absorbances. The
425 results for all the systems are presented in Figure 7. The curves for the pure inorganic salts have
426 also been measured and are included in the figure. Hereafter, we describe the effect of the various
427 acids in each of the inorganic salts as a function of RH with a special attention towards the
428 deliquescence and efflorescence behavior of the mixed particles.

429

430 1) NaCl particles

431 The deliquescence curve of NaCl/HA follows the same trend to that of pure NaCl particles:
432 no water uptake is detected until near 73% RH, where particles abruptly become liquid. Pure NaCl
433 particles deliquesce at DRH (298 K) = 75.3% (Tang and Munkelwitz 1993), a similar value.
434 However, SEM results show that particles uptake small amounts of water before sudden
435 deliquescence (as evidenced by the particle curved edges in Figure 4), although they are not enough
436 to change their size. The quantity of liquid water uptaken by NaCl particles is unaffected by the
437 presence of the HA surfactant. However, for NaCl/OA and NaCl/LA, particle deliquescence occurs
438 near to 56% RH, substantially lower than the value corresponding to pure NaCl. These results are in
439 agreement with previous reports in which a DRH of 70% was observed for NaCl particles covered
440 with OA and LA acids (Hansson et al 1998). In NaCl/OA, the particles uptake larger amounts of
441 water vapour than in pure NaCl, whereas the opposite is observed for NaCl/LA.

442 The efflorescence curves for all the three acids locate the ERH close to 40%. That value is in
443 agreement with previous works using the same technique (Cziczo and Abbatt 2000; Weis and

444 Ewing 1999) that located the ERH of pure NaCl particles at $40\pm 5\%$ RH. The curves are coincident
445 in the RH=20-60% range, but diverge towards higher RHs. For all acids particles retain larger
446 amounts of water than pure NaCl in the RH=60-95%, the quantities being in the order
447 LA>OA>HA. Also the amount of HA and OA in the particles decreases as liquid water is removed
448 from them until the ERH is reached, whereas no change in the amount of LA is observed with RH.

449

450 2) NaBr particles

451 According to Figure 7 data, NaBr/HA particles deliquesce at somewhat higher RH than pure
452 NaBr particles: liquid water in NaBr/HA particles is not detected until 50% RH. This value does not
453 change with the degree of coating, and contrasts with the value of DRH=37% for pure NaBr
454 particles (Minambres et al 2008). On the other hand, OA and LA as surfactants do not have any
455 effect on the deliquescence behavior of NaBr. The deliquescence curves are practically coincident
456 with those of pure NaBr. Also, the amount of uptaken water is similar to pure NaBr, except for OA-
457 covered particles, that uptake larger amounts of water for RH>70%. Efflorescence curves for all
458 acid surfactants are very similar to pure NaBr (ERH=23%) in the 20-60% RH (although OA retains
459 slightly more water at all RHs), but at RH>60% acid-covered particles retain higher amounts of
460 liquid water than pure NaBr (up to double for NaBr/LA at 90% RH). Thus the presence of the
461 organic covering causes water loss to happen more gradually than in the pure salt at high RHs.

462

463 3) NaI particles

464 The deliquescence curves of acid-covered NaI particles exhibit substantial differences with
465 respect to the pure salt. Whereas pure NaI particles take up water at all RHs (Minambres et al
466 2011), NaI/HA and NaI/LA particles do not uptake water until RH=16% and 21%, respectively.
467 Liquid water is not detected in NaI/OA particles until RH=75%. It can be concluded that organic
468 acid surfactant substantially retards the uptake of water in NaI particles, especially OA. The amount
469 of liquid water in HA and LA-covered particles in the RH=20-80% is higher than in pure NaI. The
470 efflorescence curve of NaI/LA is practically coincident with the pure NaI curve in the RH range
471 measured. However, the HA-covered particles lose water more gradually, retaining higher amounts
472 of water than pure NaI in the RH=30-80% range. Finally, OA-covered particles follow closely the
473 pure salt curve for RH>80%, but retain more water at lower RHs. The general tendency is that the
474 presence of acid surfactant retains more water in the particles, except for LA, which shows little
475 effect.

476

477 3.4.3. Discussion of deliquescence and efflorescence processes

478 The obtained results on the hygroscopicity of sodium halide particles covered with organic
479 acids having low water solubility show an overall complex behavior. The deliquescence curves of
480 Figure 7 indicate that the water uptake process is dependent on both the properties of inorganic salts
481 and those of the organic acids. Although the effect of the acids on the water uptake of NaBr
482 particles is small, in case of NaCl particles they produce a lowering of the DRH with respect to pure
483 salt particles. On the contrary, in NaI these acids prevent particles to uptake liquid water at low
484 RHs, unlike in pure NaI, which admits water condensation at RH as low as 6%. This retarding
485 effect is especially attributed to OA. In efflorescence a coherent behavior is observed for all
486 systems. The presence of the organic acid makes the particle to retain more water at a given RH, all
487 curves converging at the ERH.

488 The observed hygroscopic behavior can be due to several factors. The morphology of
489 particles can sometimes influence their hygroscopic behavior. However, all NaX solids have an
490 octahedral crystal structure, so all NaX dry particles are expected to be cubic. This has been verified
491 for NaCl particles by their SEM images in Figure 4. Thus we do not expect a dependence of particle
492 morphology in the hygroscopicity of different NaX salts. Another possibility is that each organic
493 acid interacts differently with each inorganic salt. Organic acids in the surface of inorganic salts will
494 tend to orientate their polar groups facing the salt surface so that ion-dipole interactions will arise
495 that will diminish the system Gibbs free energy. The polarizability of the halogen atoms increases in
496 the order Cl (14.7) < Br (21.8) < I (35.1, all in atomic units) (Lide 1994), so differences in the
497 interaction magnitude are expected. In addition, the surface of particles will become more populated
498 by anions as halide polarizability increases (Jungwirth and Tobias 2001). Our measurements show
499 that, for the same acid, the DRH increases with the polarizability of the halide anion. This behavior
500 also reflects the trend for pure NaX particles. The acid carbon chain length may also influence
501 hygroscopic behavior. In NaCl and NaBr, a longer chain produces a decrease in the DRH for the
502 HA-OA sequence (17% in NaCl, 13% in NaBr). However, further increase in the chain length (LA)
503 does not produce any effect in the DRH. On the other hand, in NaI the previous tendency does not
504 take place, and there is a noticeable increase in DRH for OA. Other effects may be responsible for
505 this behavior. It has been proposed that the structure of the monolayers formed with insoluble
506 surfactants determines their resistance towards gas uptake (Stemmler et al 2008). Fatty acids form a
507 highly ordered film in the so-called liquid condensed state, whereas in the liquid expanded state
508 they form a less ordered film and do not hinder the uptake. In that way the differences in retardation

509 in water uptake can arise from the different degrees of compression of such films (Donaldson and
510 Vaida 2006; Takahama and Russell 2011). This can be one of the reasons for the observed behavior
511 in NaI/OA particles, although we cannot verify it experimentally. Another possibility is that
512 gaseous water transport occurs through open sections of the surface that can be due to incomplete
513 packing by the organic film or to random fluctuations (Donaldson and Vaida 2006). SEM images of
514 NaCl/LA do not reveal any open section in the surface, although we cannot provide data for the rest
515 of the acids. The observed salt-specific behavior is in accordance with the observed deliquescent
516 behavior of internally mixed particles formed of sodium halide and water soluble organic acids
517 (Minambres et al 2011).

518 The hygroscopic behavior can be correlated with the spectral features of the organic acids
519 shown in Table 2, where the wavenumber and the bandwidth of the C=O band in different
520 environments are shown. The band centre wavenumbers shift in the $-6 / +10 \text{ cm}^{-1}$ range in the
521 presence of NaX salts. The bandwidth (FWHM) of the C=O vibration for the bulk acids is in the -
522 $20\text{-}29 \text{ cm}^{-1}$ range, but changes substantially for heterogeneously nucleated particles, that span the
523 $13\text{-}62 \text{ cm}^{-1}$ range (Table 2). For bulk HA, the C=O bandwidth is 20 cm^{-1} , but increases in NaX
524 particles, ranging from 27 to 40 cm^{-1} . In OA (FWHM of bulk acid is 26 cm^{-1}), the bandwidth can
525 either decrease (19 cm^{-1} in NaCl/OA) or increase (36 cm^{-1} in NaI/OA). Finally, the FWHM of
526 NaX/LA particles lies in the $19\text{-}26 \text{ cm}^{-1}$ range, taking larger values than in bulk LA (29 cm^{-1}). The
527 wavenumber shift and broadening of a spectral band may arise from a change in the internal force
528 constant of the C=O bond due to the formation of intermolecular bonds with other molecules, for
529 example hydrogen bonds with water (Kalsi 2007). These results are indicative of the effect of the
530 ionic salt environment near organic acid molecules.

531 Although it is not easy to establish clear correlations with the changes in deliquescence
532 behavior, some remarks can be outlined. For systems with NaBr the changes in the FWHM of the
533 C=O band are the smallest (except for HA/NaBr), which correlate with no change in DRH, except
534 for HA/NaBr particles, that deliquesce at 13% RH higher than in pure NaBr. For NaI mixed with an
535 organic acid, the changes in FWHM are considerable, ranging from -16 cm^{-1} in LA to $+13 \text{ cm}^{-1}$ in
536 HA (Table 2). This indicates strong ion-polar head group interaction. However, the explanation for
537 the water uptake behavior in this case can be attributed to the hydrophobic effect exerted by the
538 organic acids. It forms a barrier that prevents the entrance of gaseous water molecules inside the
539 particles. This effect is very pronounced for NaI/OA, and we have not found a satisfactory
540 explanation for it. Finally, in NaCl/organic acid systems, the opposite effect is observed, in which
541 the presence of acids slightly enhance condensation of water. This can be attributed to the ion-polar
542 group interaction that slightly lowers the Gibbs free energy of the system, favoring the uptake of

543 gaseous water molecules. The efflorescence process in NaX aqueous particles is not substantially
544 affected by the presence of the acid. As there is not an energy barrier in the efflorescence process
545 (in contrast to deliquescence), water loss takes place gradually as RH is lowered. Additionally, the
546 salting out effect of NaCl will make dissolved organic acid molecules (specially the most water
547 soluble HA) gradually move to the surface as the concentration of the salt solution increases
548 (Demou and Donaldson 2002), and will be eventually removed from the surface together with
549 water. However, as the magnitude of the salting out effect for HA is rather small (Demou and
550 Donaldson 2002), this effect is expected to contribute little in HA.

551 The results on water uptake and release, together with the release of HA from particles
552 (exemplified in Figure 6 for NaBr) give information on how the dynamics of water exchange in
553 inorganic particles is affected by the presence of a surface layer having low water solubility. In all
554 deliquescence curves in Figure 7, there is a competition for surface positions between adsorbed HA
555 and gaseous water, as indicated by the evolution of the amounts of liquid HA and water with RH
556 (or, equivalently, the relative amount of gaseous water) in Figure 6. This can be reasoned as
557 follows: in the deliquescence spectrum of Figure 6, the amount of liquid HA decreases as RH (and
558 consequently the amount of gaseous water) increases, indicating that, if we start from a dry
559 crystalline NaX particle covered with HA, gaseous water tends to displace HA molecules away
560 from the particle surface, to try to accommodate themselves on the NaX solid surface. This effect
561 can be explained as a consequence of the change in the Gibbs free energy of the system in the
562 deliquescence process: as the energetically most stable system is obtained when gaseous water
563 molecules remain near the solid NaX surface (producing deliquescence when the number of
564 gaseous water molecules reaches a given value), HA molecules will tend to be displaced from their
565 surface locations. In efflorescence, however, the observed behavior is different: removal of liquid
566 water from aqueous particles having an organic HA coating due to the decrease of RH is
567 accompanied by removal of HA from the particle surface. This effect can be explained assuming
568 that liquid HA uniformly covers the NaX aqueous particle. Water molecules exiting the particles
569 can interact with HA molecules in their surface locations and sweep them away. NaX-gaseous
570 water interactions must be stronger in NaCl than in NaBr and NaI or, alternatively, NaX-HA
571 interactions will be weaker for NaCl than for NaBr and NaI. For that reason, in NaX/HA particles,
572 HA is displaced more effectively from the surface at the DRH of pure NaCl. In NaBr and NaI,
573 however, the number density of gaseous water molecules nearby the particles at the DRH of the
574 pure inorganic particle is not enough to remove the HA cover, and a higher number of gaseous
575 water molecules (higher RH) is needed to produce particle deliquescence.

576

578 **3.5. Estimation of the relative amounts of organic acid and water in the particles**

580 The organic acid/liquid water mole ratio in the NaX particles can be obtained by applying
 581 the Beer-Lambert law (as outlined in Section 2) if \bar{A}_i and $\bar{\sigma}_i$ are known. For samples measured in
 582 the same aerosol cell, $N_{\text{org}}/N_{\text{H}_2\text{O}} = \bar{A}_{\text{org}}\bar{\sigma}_{\text{H}_2\text{O}}/\bar{A}_{\text{H}_2\text{O}}\bar{\sigma}_{\text{org}}$. The absorption cross section of liquid water
 583 has been obtained from pure water data in the 2800-3600 cm^{-1} range (Downing and Williams 1975),
 584 $\bar{\sigma}_{\text{H}_2\text{O}} = 1.3 \times 10^{-18}$ m molecule^{-1} . The absorption cross sections for liquid HA and OA have been
 585 obtained by measuring the integrated absorbance of a solution of the acid in methanol of known
 586 composition in a 150 μm long cell for liquid samples. The C=O band in the 1668-1774 cm^{-1} range
 587 was chosen to compute the integrated absorbance. The obtained values are $\bar{\sigma}_{\text{HA}} = 9.87 \times 10^{-19}$ m
 588 molecule^{-1} and $\bar{\sigma}_{\text{OA}} = 1.71 \times 10^{-19}$ m molecule^{-1} . From these data, the average $N_{\text{HA}}/N_{\text{H}_2\text{O}}$ and
 589 $N_{\text{OA}}/N_{\text{H}_2\text{O}}$ ratios have been calculated for the various salts at several RHs. The results appear in
 590 Figure 8. The obtained results indicate that $N_{\text{HA}}/N_{\text{H}_2\text{O}}$ values are comprised in the 0.1-0.6 range for
 591 RH in the 30-98% interval, the lowest values corresponding to the highest RHs. In contrast, the
 592 $N_{\text{OA}}/N_{\text{H}_2\text{O}}$ quotient spans from 0.2 to 1.9 (for RHs in the 40-96% range), when again the highest
 593 values correspond to the lowest RH conditions. The highest $N_{\text{OA}}/N_{\text{H}_2\text{O}}$ ratio (1.9) is obtained for NaI
 594 efflorescing particles. The results in Fig. 8 indicate that, in general, OA-covered particles tend to
 595 displace liquid water more efficiently than HA-covered particles.

596 The spectroscopic results indicate that gaseous HA, OA and LA easily nucleate onto dry and
 597 aqueous NaX particles. The amount of acid uptaken increases with the temperature of the oven.
 598 Additionally, SEM images of NaCl particles with LA show NaCl particle aggregates, indicating that
 599 they are "glued" by lauric acid. However, SEM images provide no visual evidence of the presence
 600 of an organic surfactant, so we can conclude that the cover must be much thinner than the size of
 601 the salt particles. Although in principle it is possible that part of the surfactant evaporates before
 602 particles are covered with gold, LA has a low vapor pressure (2.2×10^{-5} mbar, see Table 1), so we do
 603 not expect acid evaporation to alter the sample appreciably. A rough higher limit for the cover
 604 thickness can be set at 20 nm, which is the resolution of the SEM images. This estimate can be
 605 compared with HA and OA cover thickness on aqueous particles, calculated assuming that liquid
 606 HA or OA arrange in a hydrophobic organic layer in the surface of an aqueous particle, according to
 607 one proposed model (Ellison et al 1999), and taking into account the spectrally measured relative

608 proportions of water and organic acid. The volume of a spherical aqueous particle of radius R will
609 be $V_{\text{H}_2\text{O}} = (4/3)\pi R^3$, whereas the volume of liquid organic coating of thickness r , assuming uniform
610 coverage, can be written as $V_{\text{org}} = (4/3)\pi[(R+r)^3 - R^3]$. On the other hand, $V_{\text{org}}/V_{\text{H}_2\text{O}} =$
611 $N_{\text{org}}\rho_{\text{H}_2\text{O}}/(N_{\text{H}_2\text{O}}\rho_{\text{org}})$, where ρ stands for density. As the $N_{\text{org}}/N_{\text{H}_2\text{O}}$ ratios have been determined
612 previously, from the previous equations we can obtain r in terms of the aqueous particle radius R :

$$613 \quad r/R = [1 + N_{\text{org}}\rho_{\text{H}_2\text{O}}/(N_{\text{H}_2\text{O}}\rho_{\text{org}})]^{1/3} - 1$$

614 For typical values of $N_{\text{HA}}/N_{\text{H}_2\text{O}} = 0.1, 0.3$ and 0.6 , $r/R = 0.035, 0.098$ and 0.181 ,
615 respectively, indicating that the thickness of the organic layer increases roughly linearly with the
616 number of molecules of liquid HA. For example, if $N_{\text{HA}}/N_{\text{H}_2\text{O}} = 0.3$ and $R = 0.3 \mu\text{m}$ (roughly
617 corresponding to NaCl particles appearing in Figure 4c), the HA coating thickness yields an
618 estimation of $r = 29 \text{ nm}$ for a particle coated with HA. This value can be compared with the upper
619 limit of 20 nm estimated for the cover thickness in the LA/NaCl system. The former HA-coating
620 thickness is much larger than the estimated thickness of a monolayer, which is roughly 0.3 nm ,
621 assuming a completely extended linear chain and taking into account an average C-C bond length of
622 0.077 nm . However, we cannot affirm whether the particles are uniformly covered. Previous
623 investigations indicate that the degree of insoluble acid coverage do not substantially alter DRH.
624 Complete coverage of inorganic particles by fatty acids had no dramatic effect on NaCl particle
625 DRH (Andrews and Larson 1993). On the other hand, DRH of ammonium sulfate was only slightly
626 lowered for oleic acid thickness up to 109 nm (Najera and Horn 2009), much bigger than our
627 estimated thickness of around 30 nm . No variations in DRH with acid covering thickness were
628 observed in this work.

629

630

631 **4. CONCLUSIONS AND ATMOSPHERIC IMPLICATIONS**

632

633 This work studied the effect of a surfactant layer of hexanoic, octanoic and lauric acid,
634 which are present in the Earth's troposphere, on the hygroscopic properties of sodium halide
635 submicrometer particles, which are constituents of sea salt aerosol. Infrared extinction spectroscopy
636 together with particle counting and visualizing techniques allowed us to detect the formation of
637 homogeneously and heterogeneously nucleated particles and the variation of their composition in

638 the presence of variable amounts of gaseous water, leading to the processes of deliquescence and
639 efflorescence.

640 It was found that the hygroscopic properties of sodium halide particles covered with
641 hexanoic, octanoic or lauric acid change both with the nature of the inorganic salt and the
642 carboxylic acid. The DRH of NaCl aerosol experiences a moderate shift with the nature of the
643 organic acid covering the particles. The deliquescence of NaCl/OA and NaCl/LA systems occurs
644 near RH=56%, below the DRH of pure NaCl. On the other hand, NaBr covered particles do not
645 substantially alter their water uptake behavior respect to pure salt particles for OA and LA
646 surfactants, but the DRH of NaBr /HA particles is about 13% higher than that of pure NaBr. Finally,
647 organic acid covering on solid NaI particles acts as a barrier to water uptake; NaI particles
648 deliquesce near 16% and 21% RH when coated with hexanoic and lauric acid, respectively, but the
649 DRH of NaI/OA particles rises to a value higher than 60%. The general consequence is that the
650 water uptake behavior of sodium halide particles coated with organic acids is dependent on the
651 nature of the anion and the carboxylic acid. This is in accordance with former studies of sodium
652 halides with succinic acid, which showed a salt-specific behavior. Consequently, although it is
653 customary to extrapolate the water uptake behavior of NaCl particles to sea salt aerosol due to the
654 predominance of this species in marine salt, the detailed picture can be more complex.

655 Regarding efflorescence process, the obtained results indicated that the overall effect of the
656 organic acid cover is to retain higher amounts of water at RH in the 60-90% range with respect to
657 pure NaX particles. In NaCl particles the longer chain acid (LA) achieved the highest water
658 retention, while the shortest one (HA) provided the lowest. All acids act similarly in NaBr aqueous
659 particles, whereas in aqueous NaI particles OA is the acid that produces higher water retention at
660 RH in the 60-90% range. The results showed that this barrier effect is dependent on the nature of
661 the organic acid, and can have important consequences for the troposphere, as the organic species
662 can determine the amount of liquid water in the particles and their phase at a given RH. Based on
663 our data, there is no simple correlation between water uptake or crystallization processes in coated
664 salt particles and the length of the carbonated chain in the carboxylic acid. The complex behavior in
665 hygroscopic properties in the different salts cannot be easily attributed to a single effect, and the
666 results point to more specific ion-molecule interactions in the NaX/organic acid/H₂O systems or to
667 the structure of the organic film on the particle.

668 SEM measurements and data deduced from the infrared absorbance spectra indicated that
669 the covering thickness of the obtained salt particles is compatible with an average value of 30 nm.
670 SEM images showed that the effect of lauric acid on NaCl is to agglomerate salt particles,

671 producing bigger effective particles. It was not possible to observe this effect with the other acids,
672 due to experimental inconveniences.

673 Several consequences for the atmosphere can be driven from this study: as bromine and
674 iodine ions tend to segregate to the surface of marine aerosol particles, and the effect of fatty acids
675 on them can be different as compared to the more abundant NaCl species, this may influence the
676 surface properties of the particles not usually taken into account in the models. At a given value of
677 ambient relative humidity, sea salt particles may have an outer core in which NaBr and NaI are
678 more abundant, and if an organic layer having a low water solubility is present, the interactions of
679 the organic compound will predominantly take place with bromide and iodide ions. At given
680 conditions of relative humidity in the atmosphere, liquid water amounts and phase of sea-salt
681 particle outer core may vary regard to the expected behavior of pure NaCl particles. This has
682 consequences in the heterogeneous processes taking place between particles and atmospheric gases,
683 such as gas uptake and chemical reactivity.

684

685

686 **ACKNOWLEDGMENTS**

687 The authors are grateful to Ministerio de Ciencia e Innovación (Madrid) for grant-in-aids
688 (CGL2011-22441 and Consolider CSD-2007-00013), to Gobierno Vasco/Eusko Jaurlaritza
689 (Vitoria-Gasteiz) for a Consolidated Research Group grant (IT520-10), and UPV/EHU for
690 UFI11/23, SEM facilities (SGI/IZO-SGIker) and general support. L.M. thanks UPV/EHU for a
691 postdoctoral research grant. We are grateful to Dr. Cristina Gutiérrez from UPV/EHU for the use of
692 the butanol CPC.

693

694

695 **REFERENCES**

696

- 697 Abbatt, J., Broekhuizen, K., and Pradeep Kumar, P. 2005. Cloud condensation nucleus activity of
698 internally mixed ammonium sulfate/organic acid aerosol particles. *Atmos. Environ.* 39:4767-4778.
- 699 Andreae, M., and Rosenfeld, D. 2008. Aerosol–cloud–precipitation interactions. Part 1. The nature
700 and sources of cloud-active aerosols. *Earth-Sci.Rev.* 89:13-41.
- 701 Andrews, E., and Larson, S. M. 1993. Effect of Surfactant Layers on the Size Changes of Aerosol-
702 Particles as a Function of Relative-Humidity. *Environ.Sci.Technol.* 27.
- 703 Ault, A. P., Moffet, R. C., Baltusaitis, J., Collins, D. B., Ruppel, M. J., Cuadra-Rodriguez, L. A.,
704 Zhao, D., Guasco, T. L., Ebben, C. J., and Geiger, F. M. 2013. Size-dependent changes in sea spray
705 aerosol composition and properties with different seawater conditions. *Environ.Sci.Technol.*
706 47:5603-5612.
- 707 Baker, A. R. 2005. Marine aerosol iodine chemistry: The importance of soluble organic iodine.
708 *Environ. Chem.* 2.
- 709 Bialek, J., Dall'Osto, M., Monahan, C., Beddows, D., and O'Dowd, C. 2012. On the contribution of
710 organics to the North East Atlantic aerosol number concentration. *Environ. Res. Lett.* 7:044013.
- 711 Carpenter, L. J. 2003. Iodine in the marine boundary layer. *Chem.Rev.* 103:4953-4962.
- 712 Carslaw, K., Boucher, O., Spracklen, D., Mann, G., Rae, J., Woodward, S., and Kulmala, M. 2010.
713 A review of natural aerosol interactions and feedbacks within the Earth system. *Atmos. Chem.*
714 *Phys.* 10:1701-1737.
- 715 Cavalli, F., Facchini, M. C., Decesari, S., Mircea, M., Emblico, L., Fuzzi, S., Ceburnis, D., Yoon,
716 Y. J., O'Dowd, C. D., Putaud, J. P., and Dell'Acqua, A. 2004. Advances in characterization of size-
717 resolved organic matter in marine aerosol over the North Atlantic. *J. Geophys. Res. Atmos.*
718 109:D24215.
- 719 Chakraborty, P., and Zachariah, M. R. 2008. Sticking coefficient and processing of water vapor on
720 organic-coated nanoaerosols. *J. Phys. Chem. A.* 112.
- 721 Chuang, P. Y. 2003. Measurement of the timescale of hygroscopic growth for atmospheric aerosols.
722 *J. Geophys. Res. Atmos.* 108:4282.
- 723 Ciobanu, V. G., Marcolli, C., Krieger, U. K., Weers, U., and Peter, T. 2009. Liquid– liquid phase
724 separation in mixed organic/inorganic aerosol particles. *J. Phys. Chem. A.* 113:10966-10978.
- 725 Cwiertny, D. M., Young, M. A., and Grassian, V. H. 2008. Chemistry and Photochemistry of
726 Mineral Dust Aerosol*. *Annu.Rev.Phys.Chem.* 59:27-51.
- 727 Cziczo, D., and Abbatt, J. 2000. Infrared observations of the response of NaCl, MgCl₂, NH₄HSO₄,
728 and NH₄NO₃ aerosols to changes in relative humidity from 298 to 238 K. *J. Phys. Chem. A.*
729 104:2038-2047.

- 730 D O'Dowd, C., and De Leeuw, G. 2007. Marine aerosol production: a review of the current
731 knowledge. *Philos. Trans. R. Soc. London, Ser. A.* 365:1753-1774.
- 732 Dall'Osto, M., Ceburnis, D., Martucci, G., Bialek, J., Dupuy, R., Jennings, S., Berresheim, H.,
733 Wenger, J., Healy, R., and Facchini, M. 2010. Aerosol properties associated with air masses
734 arriving into the North East Atlantic during the 2008 Mace Head EUCAARI intensive observing
735 period: an overview. *Atmos. Chem. Phys.* 10.
- 736 Davies, J. F., Miles, R. E., Haddrell, A. E., and Reid, J. P. 2013. Influence of organic films on the
737 evaporation and condensation of water in aerosol. *PNAS.* 110:8807-8812.
- 738 Demou, E., and Donaldson, D. J. 2002. Adsorption of atmospheric gases at the air-water interface.
739 4: The influence of salts. *J. Phys. Chem. A.* 106.
- 740 Dennis-Smith, B. J., Hanford, K. L., Kwamena, N. A., Miles, R. E. H., and Reid, J. P. 2012.
741 Phase, Morphology, and Hygroscopicity of Mixed Oleic Acid/Sodium Chloride/Water Aerosol
742 Particles before and after Ozonolysis. *J. Phys. Chem. A.* 116.
- 743 Donaldson, D. J., and Vaida, V. 2006. The influence of organic films at the air-aqueous boundary
744 on atmospheric processes. *Chem.Rev.* 106.
- 745 Downing, H. D., and Williams, D. 1975. Optical constants of water in the infrared. *J. Geophys. Res.*
746 80:1656-1661.
- 747 Duce, R., Mohnen, V., Zimmerman, P., Grosjean, D., Cautreels, W., Chatfield, R., Jaenicke, R.,
748 Ogren, J., Pellizzari, E., and Wallace, G. 1983. Organic material in the global troposphere.
749 *Rev.Geophys.* 21:921-952.
- 750 Ebben, C. J., Ault, A. P., Ruppel, M. J., Ryder, O. S., Bertram, T. H., Grassian, V. H., Prather, K.
751 A., and Geiger, F. M. 2013. Size-Resolved Sea Spray Aerosol Particles Studied by Vibrational Sum
752 Frequency Generation. *J. Phys. Chem. A.* 117:6589-6601.
- 753 Ellison, G. B., Tuck, A. F., and Vaida, V. 1999. Atmospheric processing of organic aerosols. *J.*
754 *Geophys. Res. Atmos.* 104.
- 755 Fierz-Schmidhauser, R., Zieger, P., Vaishya, A., Monahan, C., Bialek, J., O'Dowd, C., Jennings, S.,
756 Baltensperger, U., and Weingartner, E. 2010. Light scattering enhancement factors in the marine
757 boundary layer (Mace Head, Ireland). *J. Geophys. Res. Atmos.* 115.
- 758 Finlayson-Pitts, B. J. 2009. Reactions at surfaces in the atmosphere: integration of experiments and
759 theory as necessary (but not necessarily sufficient) for predicting the physical chemistry of aerosols.
760 *PCCP.* 11:7760-7779.
- 761 Finlayson-Pitts, B. 2003. The tropospheric chemistry of sea salt: A molecular-level view of the
762 chemistry of NaCl and NaBr. *Chem.Rev.* 103:4801-4822.
- 763 Firanescu, G., Hermsdorf, D., Ueberschaer, R., and Signorell, R. 2006. Large molecular aggregates:
764 From atmospheric aerosols to drug nanoparticles. *PCCP.* 8:4149-4165.
- 765 Freney, E. J., Martin, S. T., and Buseck, P. R. 2009. Deliquescence and efflorescence of potassium
766 salts relevant to biomass-burning aerosol particles. *Aerosol Sci. Technol.* 43:799-807.

- 767 Frinak, E. K., and Abbatt, J. P. D. 2006. Br(2) production from the heterogeneous reaction of gas-
768 phase OH with aqueous salt solutions: Impacts of acidity, halide concentration, and organic
769 surfactants. *J. Phys. Chem. A.* 110.
- 770 Gadermann, M., Preston, T. C., Troster, C., and Signorell, R. 2008. Characterization of palmitic and
771 lauric acid aerosols from rapid expansion of supercritical CO₂ solutions. *Mol.Phys.* 106:945-953.
- 772 Gantt, B., and Meskhidze, N. 2013. The physical and chemical characteristics of marine primary
773 organic aerosol: a review. *Atmos. Chem. Phys.* 13:3979-3996.
- 774 Garland, R., Wise, M., Beaver, M., DeWitt, H., Aiken, A., Jimenez, J., and Tolbert, M. 2005.
775 Impact of palmitic acid coating on the water uptake and loss of ammonium sulfate particles. *Atmos.*
776 *Chem. Phys.* 5:1951-1961.
- 777 Garland, E. R., Rosen, E. P., Clarke, L. I., and Baer, T. 2008. Structure of submonolayer oleic acid
778 coverages on inorganic aerosol particles: evidence of island formation. *PCCP.* 10.
- 779 Ghosal, S., Brown, M. A., Bluhm, H., Krisch, M. J., Salmeron, M., Jungwirth, P., and Hemminger,
780 J. C. 2008. Ion Partitioning at the Liquid/Vapor Interface of a Multicomponent Alkali Halide
781 Solution: A Model for Aqueous Sea Salt Aerosols. *J. Phys. Chem. A.* 112.
- 782 Gill, P., Graedel, T., and Weschler, C. 1983. Organic films on atmospheric aerosol particles, fog
783 droplets, cloud droplets, raindrops, and snowflakes. *Rev.Geophys.* 21:903-920.
- 784 Hämeri, K., Rood, M., and Hansson, H. 1992. Hygroscopic properties of a NaCl aerosol coated with
785 organic compounds. *J.Aerosol Sci.* 23:437-440.
- 786 Hansson, H. C., Rood, M. J., Koloutsou-Vakakis, S., Hameri, K., Orsini, D., and Wiedensohler, A.
787 1998. NaCl aerosol particle hygroscopicity dependence on mixing with organic compounds.
788 *J.Atmos.Chem.* 31.
- 789 Hayase, S., Yabushita, A., Kawasaki, M., Enami, S., Hoffmann, M. R., and Colussi, A. J. 2011.
790 Weak Acids Enhance Halogen Activation on Atmospheric Water's Surfaces. *J. Phys. Chem. A.* 115.
- 791 Hinds, W. C. 1998. *Aerosol technology :properties, behavior, and measurement of airborne*
792 *particles.* John Wiley & Sons.
- 793 Hunt, S. W., Roeselova, M., Wang, W., Wingen, L. M., Knipping, E. M., Tobias, D. J., Dabdub, D.,
794 and Finlayson-Pitts, B. J. 2004. Formation of molecular bromine from the reaction of ozone with
795 deliquesced NaBr aerosol: Evidence for interface chemistry. *J. Phys. Chem. A.* 108.
- 796 IPCC. 2013. *Climate Change 2013: The Physical Science Basis. Contribution of Working Group I*
797 *to the Fifth Assessment Report of the Intergovernmental Panel on Climate Change. Pages 571-658*
798 *in: Clouds and Aerosols. Anonymous . Cambridge University Press: Cambridge, United Kingdom*
799 *and New York, NY, USA.*
- 800 Jungwirth, P., and Tobias, D. J. 2001. Molecular structure of salt solutions: a new view of the
801 interface with implications for heterogeneous atmospheric chemistry. *J. Phys. Chem. B.* 105:10468-
802 10472.
- 803 Kalsi, P. 2007. *Spectroscopy of organic compounds.* New Age International.

- 804 Kleefeld, S., Hoffer, A., Krivacsy, Z., and Jennings, S. 2002. Importance of organic and black
805 carbon in atmospheric aerosols at Mace Head, on the west coast of Ireland (53 19' N, 9 54' W).
806 *Atmos. Environ.* 36:4479-4490.
- 807 Krueger, B. J., Grassian, V. H., Iedema, M. J., Cowin, J. P., and Laskin, A. 2003. Probing
808 heterogeneous chemistry of individual atmospheric particles using scanning electron microscopy
809 and energy-dispersive X-ray analysis. *Anal. Chem.* 75:5170-5179.
- 810 Kwamena, N. - A., Buajareern, J., and Reid, J. P. 2010. Equilibrium Morphology of Mixed
811 Organic/Inorganic/Aqueous Aerosol Droplets: Investigating the Effect of Relative Humidity and
812 Surfactants. *J. Phys. Chem. A.* 114.
- 813 Lewis, R., and Schwartz, E. 2004. Sea salt aerosol production: mechanisms, methods,
814 measurements and models—a critical review. American Geophysical Union.
- 815 Lide, D. R. 1994. *CRC handbook of chemistry and physics.* CRC press: Boca Raton, FL.
- 816 Limbeck, A., and Puxbaum, H. 1999. Organic acids in continental background aerosols.
817 *Atmos. Environ.* 33:1847-1852.
- 818 Ma, X., Chakraborty, P., Henz, B. J., and Zachariah, M. R. 2011. Molecular dynamic simulation of
819 dicarboxylic acid coated aqueous aerosol: structure and processing of water vapor. *PCCP.* 13:9374-
820 9384.
- 821 Martin, S. T. 2000. Phase transitions of aqueous atmospheric particles. *Chem. Rev.* 100:3403-3453.
- 822 Metzger, S., and Lelieveld, J. 2007. Reformulating atmospheric aerosol thermodynamics and
823 hygroscopic growth into fog, haze and clouds. *Atmos. Chem. Phys.* 7:3163-3193.
- 824 Middlebrook, A. M., Murphy, D. M., and Thomson, D. S. 1998. Observations of organic material in
825 individual marine particles at Cape Grim during the First Aerosol Characterization Experiment
826 (ACE 1). *J. Geophys. Res.* 103:16475-16,483.
- 827 Mikhailov, E., Vlasenko, S., Rose, D., and Pöschl, U. 2013. Mass-based hygroscopicity parameter
828 interaction model and measurement of atmospheric aerosol water uptake. *Atmos. Chem. Phys.*
829 13:717-740.
- 830 Minambres, L., Mendez, E., Sanchez, M. N., Castano, F., and Basterretxea, F. J. 2011. Water
831 uptake properties of internally mixed sodium halide and succinic acid particles. *Atmos. Environ.* 45.
- 832 Minambres, L., Sanchez, M. N., Castano, F., and Basterretxea, F. J. 2010. Hygroscopic Properties
833 of Internally Mixed Particles of Ammonium Sulfate and Succinic Acid Studied by Infrared
834 Spectroscopy. *J. Phys. Chem. A.* 114.
- 835 Minambres, L., Sanchez, M. N., Castano, F., and Basterretxea, F. J. 2008. Infrared spectroscopic
836 properties of sodium bromide aerosols. *J. Phys. Chem. A.* 112.
- 837 Mochida, M., Kitamori, Y., Kawamura, K., Nojiri, Y., and Suzuki, K. 2002. Fatty acids in the
838 marine atmosphere: Factors governing their concentrations and evaluation of organic films on sea-
839 salt particles. *J. Geophys. Res. Atmos.* 107:4325.

- 840 Najera, J. J., and Horn, A. B. 2009. Infrared spectroscopic study of the effect of oleic acid on the
841 deliquescence behaviour of ammonium sulfate aerosol particles. *PCCP*. 11.
- 842 O'Dowd, C. D., Facchini, M. C., Cavalli, F., Ceburnis, D., Mircea, M., Decesari, S., Fuzzi, S.,
843 Yoon, Y. J., and Putaud, J. 2004. Biogenically driven organic contribution to marine aerosol.
844 *Nature*. 431:676-680.
- 845 O'Dowd, C. D., Jimenez, J. L., Bahreini, R., Flagan, R. C., Seinfeld, J. H., Hämeri, K., Pirjola, L.,
846 Kulmala, M., Jennings, S. G., and Hoffmann, T. 2002. Marine aerosol formation from biogenic
847 iodine emissions. *Nature*. 417:632-636.
- 848 O'Dowd, C. D., Smith, M. H., Consterdine, I. E., and Lowe, J. A. 1997. Marine aerosol, sea-salt,
849 and the marine sulphur cycle: A short review. *Atmos. Environ.* 31:73-80.
- 850 Ovadnevaite, J., O'Dowd, C., Dall'Osto, M., Ceburnis, D., Worsnop, D. R., and Berresheim, H.
851 2011b. Detecting high contributions of primary organic matter to marine aerosol: A case study.
852 *Geophys. Res. Lett.* 38.
- 853 Ovadnevaite, J., Ceburnis, D., Martucci, G., Bialek, J., Monahan, C., Rinaldi, M., Facchini, M. C.,
854 Berresheim, H., Worsnop, D. R., and O'Dowd, C. 2011a. Primary marine organic aerosol: A
855 dichotomy of low hygroscopicity and high CCN activity. *Geophys. Res. Lett.* 38.
- 856 Prather, K. A., Bertram, T. H., Grassian, V. H., Deane, G. B., Stokes, M. D., DeMott, P. J.,
857 Aluwihare, L. I., Palenik, B. P., Azam, F., and Seinfeld, J. H. 2013. Bringing the ocean into the
858 laboratory to probe the chemical complexity of sea spray aerosol. *PNAS*. 110:7550-7555.
- 859 Putaud, J., Van Dingenen, R., Mangoni, M., Virkkula, A., Raes, F., Maring, H., Prospero, J.,
860 Swietlicki, E., Berg, O., and Hillamo, R. 2000. Chemical mass closure and assessment of the origin
861 of the submicron aerosol in the marine boundary layer and the free troposphere at Tenerife during
862 ACE-2. *Tellus Ser. B*. 52:141-168.
- 863 Quinn, P., and Bates, T. 2011. The case against climate regulation via oceanic phytoplankton
864 sulphur emissions. *Nature*. 480:51-56.
- 865 Read, K. A., Mahajan, A. S., Carpenter, L. J., Evans, M. J., Faria, B. V., Heard, D. E., Hopkins, J.
866 R., Lee, J. D., Moller, S. J., and Lewis, A. C. 2008. Extensive halogen-mediated ozone destruction
867 over the tropical Atlantic Ocean. *Nature*. 453:1232-1235.
- 868 Reid, J. P., Dennis-Smith, B. J., Kwamena, N. A., Miles, R. E., Hanford, K. L., and Homer, C. J.
869 2011. The morphology of aerosol particles consisting of hydrophobic and hydrophilic phases:
870 hydrocarbons, alcohols and fatty acids as the hydrophobic component. *PCCP*. 13:15559-15572.
- 871 Rinaldi, M., Decesari, S., Finessi, E., Giulianelli, L., Carbone, C., Fuzzi, S., O'Dowd, C. D.,
872 Ceburnis, D., and Facchini, M. C. 2010. Primary and secondary organic marine aerosol and oceanic
873 biological activity: Recent results and new perspectives for future studies. *Adv. Meteor.* 2010.
- 874 Robinson, C. B., Schill, G. P., Zarzana, K. J., and Tolbert, M. A. 2013. Impact of Organic Coating
875 on Optical Growth of Ammonium Sulfate Particles. *Environ. Sci. Technol.* 47:13339-13346.
- 876 Rossi, M. J. 2003. Heterogeneous reactions on salts. *Chem. Rev.* 103.

- 877 Rouviere, A., and Ammann, M. 2010. The effect of fatty acid surfactants on the uptake of ozone to
878 aqueous halogenide particles. *Atmos. Chem. Phys.* 10:11489-11500.
- 879 Rubasinghege, G., Ogden, S., Baltrusaitis, J., and Grassian, V. H. 2013. Heterogeneous Uptake and
880 Adsorption of Gas-Phase Formic Acid on Oxide and Clay Particle Surfaces: The Roles of Surface
881 Hydroxyl Groups and Adsorbed Water in Formic Acid Adsorption and the Impact of Formic Acid
882 Adsorption on Water Uptake. *J. Phys. Chem. A.* 117:11316-11327.
- 883 Safar, M., Bertrand, D., Robert, P., Devaux, M., and Genot, C. 1994. Characterization of edible oils,
884 butters and margarines by Fourier transform infrared spectroscopy with attenuated total reflectance.
885 *J. Am. Oil Chem. Soc.* 71:371-377.
- 886 Saiz-Lopez, A., Plane, J., Mahajan, A., Anderson, P., Bauguitte, S., Jones, A., Roscoe, H., Salmon,
887 R., Bloss, W., and Lee, J. 2008. On the vertical distribution of boundary layer halogens over coastal
888 Antarctica: implications for O₃, HO_x, NO_x and the Hg lifetime. *Atmos. Chem. Phys.* 8:887-900.
- 889 Samy, S., Mazzoleni, L. R., Mishra, S., Zielinska, B., and Hallar, A. G. 2010. Water-soluble
890 organic compounds at a mountain-top site in Colorado, USA. *Atmos. Environ.* 44:1663-1671.
- 891 Schauer, J. J., Kleeman, M. J., Cass, G. R., and Simoneit, B. R. 2002. Measurement of emissions
892 from air pollution sources. 4. C1-C27 organic compounds from cooking with seed oils.
893 *Environ. Sci. Technol.* 36:567-575.
- 894 Schauer, J. J., Kleeman, M. J., Cass, G. R., and Simoneit, B. R. 1999. Measurement of emissions
895 from air pollution sources. 1. C1 through C29 organic compounds from meat charbroiling.
896 *Environ. Sci. Technol.* 33:1566-1577.
- 897 Soule, M. C. K., Blower, P. G., and Richmond, G. L. 2007. Effects of atmospherically important
898 solvated ions on organic acid adsorption at the surface of aqueous solutions. *J Phys Chem B.* 111.
- 899 Stemmler, K., Vlasenko, A., Guimbaud, C., and Ammann, M. 2008. The effect of fatty acid
900 surfactants on the uptake of nitric acid to deliquesced NaCl aerosol. *Atmos. Chem. Phys.* 8:5127-
901 5141.
- 902 Sun, L., Hede, T., Tu, Y., Leck, C., and Ågren, H. 2013. Combined Effect of Glycine and Sea Salt
903 on Aerosol Cloud Droplet Activation Predicted by Molecular Dynamics Simulations. *J. Phys.*
904 *Chem. A.* 117:10746-10752.
- 905 Sun, L., Li, X., Hede, T., Tu, Y., Leck, C., and Ågren, H. 2012. Molecular dynamics simulations of
906 the surface tension and structure of salt solutions and clusters. *J. Phys. Chem. B.* 116:3198-3204.
- 907 Tabazadeh, A. 2005. Organic aggregate formation in aerosols and its impact on the
908 physicochemical properties of atmospheric particles. *Atmos. Environ.* 39:5472-5480.
- 909 Takahama, S., and Russell, L. 2011. A molecular dynamics study of water mass accommodation on
910 condensed phase water coated by fatty acid monolayers. *J. Geophys. Res. Atmos.* 116.
- 911 Tang, I. N., and Munkelwitz, H. R. 1993. Composition and Temperature-Dependence of the
912 Deliquescence Properties of Hygroscopic Aerosols. *Atmos. Environ. Part A.* 27.

- 913 Tervahattu, H., Hartonen, K., Kerminen, V. M., Kupiainen, K., Aarnio, P., Koskentalo, T., Tuck, A.
914 F., and Vaida, V. 2002. New evidence of an organic layer on marine aerosols. *J. Geophys. Res.*
915 *Atmos.* 107:4053.
- 916 Vaishya, A., Ovadnevaite, J., Bialek, J., Jennings, S. G., Ceburnis, D., and O'Dowd, C. D. 2013.
917 Bistable effect of organic enrichment on sea spray radiative properties. *Geophys.Res.Lett.* 40:6395-
918 6398.
- 919 Veghte, D. P., Altaf, M. B., and Freedman, M. A. 2013. Size Dependence of the Structure of
920 Organic Aerosol. *J.Am.Chem.Soc.* 135:16046-16049.
- 921 Von Glasow, R. 2008. Atmospheric chemistry - Sun, sea and ozone destruction. *Nature.* 453.
- 922 Wagner, J., Andrews, E., and Larson, S. M. 1996. Sorption of vapor phase octanoic acid onto
923 deliquescent salt particles. *J. Geophys. Res.* 101:19533-19,540.
- 924 Weis, D. D., and Ewing, G. E. 1996. Infrared spectroscopic signatures of (NH₄)₂SO₄ aerosols. *J.*
925 *Geophys. Res.* 101:18709-18,720.
- 926 Weis, D. D., and Ewing, G. E. 1999. Water content and morphology of sodium chloride aerosol
927 particles. *J. Geophys. Res. Atmos.* 104:21275-21285.
- 928 Wise, M. E., Baustian, K. J., Koop, T., Freedman, M. A., Jensen, E. J., and Tolbert, M. A. 2012.
929 Depositional ice nucleation onto crystalline hydrated NaCl particles: a new mechanism for ice
930 formation in the troposphere. *Atmos. Chem. Phys.* 12:1121-1134.
- 931 Yassaa, N., Meklati, B. Y., Brancaleoni, E., Frattoni, M., and Ciccioli, P. 2001. Polar and non-polar
932 volatile organic compounds (VOCs) in urban Algiers and saharian sites of Algeria. *Atmos.Environ.*
933 35:787-801.
- 934 Zangmeister, C. D., Turner, J. A., and Pemberton, J. E. 2001. Segregation of NaBr in NaBr/NaCl
935 crystals grown from aqueous solutions: Implications for sea salt surface chemistry.
936 *Geophys.Res.Lett.* 28.
- 937
938

939 **FIGURE CAPTIONS**

940
941

942 **Figure 1:** A diagram of the experimental setup. RH is measured by a thermohygrometer with the
943 sensor placed at the exit of the aerosol flow cell. The heating cell where the organic acid sample is
944 located can be heated by two independent resistors at two different temperatures: T_1 (75-100°C) in
945 the central part of the tube and T_2 (60-90°C) at the exit arm.

946

947 **Figure 2:** Representative particle size distributions of dry NaCl aerosol. A has been obtained by
948 imaging particles deposited on a glass slide by SEM technique and counting them with the ImageJ
949 software [rsbweb.nih.gov/ij/]. B and C have been obtained by sizing particles by an aerodynamic
950 particle spectrometer; pure NaCl particles (B) and heterogeneously nucleated particles with
951 hexanoic particles (C) are shown.

952

953 **Figure 3:** Infrared extinction spectra of HA (A), OA (B) and LA (C) in different conditions: bottom
954 spectra are from bulk phase acid; medium spectra corresponds to homogeneously nucleated acid
955 particles; upper spectra are from heterogeneously nucleated acids onto NaCl particles. In all cases,
956 the upper spectra have been increased for clarity (increasing factor: \times Number)

957

958 **Figure 4:** SEM images of: (a) pure NaCl particles; (b) pure LA particles; (c) NaCl particles covered
959 with LA.

960

961 **Figure 5:** Infrared spectra of NaBr particles after passing through the heated reservoir containing
962 OA and exposed to different RHs.

963

964 **Figure 6:** Spectra showing the evolution of the infrared absorption intensity of the C=O band of
965 hexanoic acid near 1700 cm^{-1} with RH in NaBr particles in deliquescence and efflorescence mode.
966 Also the shaded region indicates the selected area for measuring liquid water abundance in the
967 particles (see text).

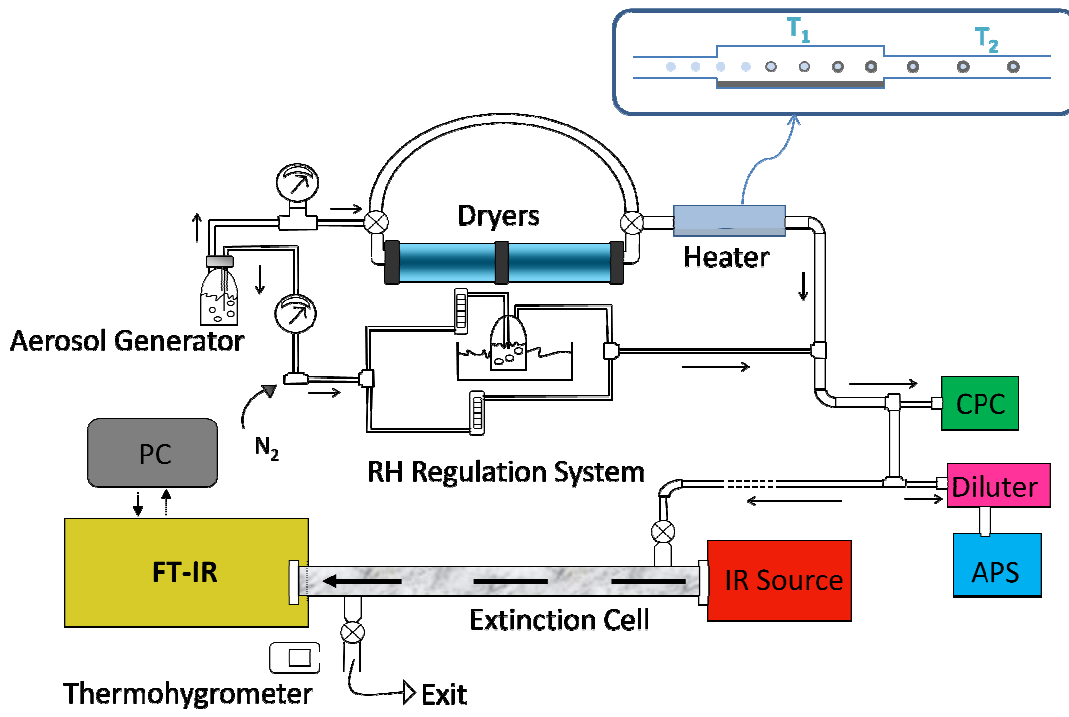
968

969 **Figure 7:** Deliquescence and efflorescence curves of NaX (X = Cl, Br, I) particles covered with
970 HA, OA and LA. The curves for the pure inorganic salts are shown by lines. Left and right panels
971 show deliquescence and efflorescence curves, respectively. Liquid water mass is calculated as
972 explained in Section 2.

973

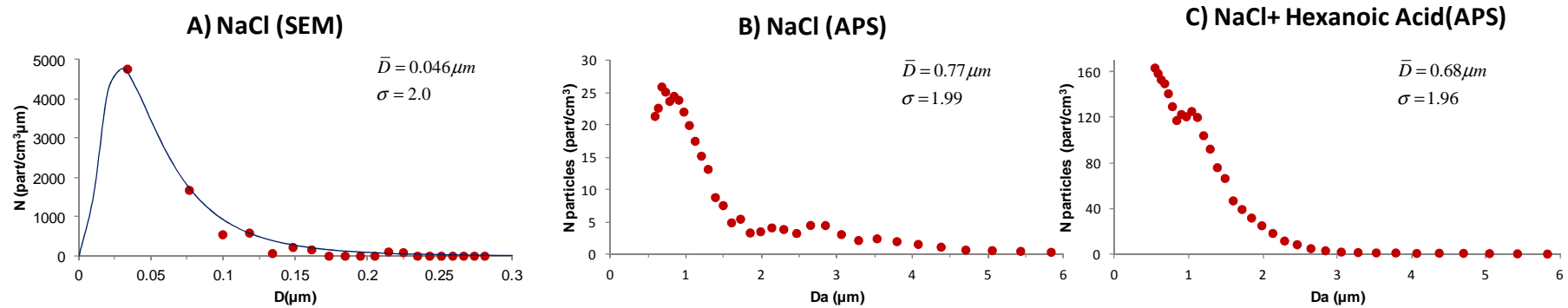
974 **Figure 8:** $N_{\text{HA}}/N_{\text{H}_2\text{O}}$ and $N_{\text{OA}}/N_{\text{H}_2\text{O}}$ mole ratios in heterogeneously coated particles at various
975 relative humidities in deliquescence and efflorescence conditions. “del” and “effl” stand for
976 deliquescence and efflorescence. “RH” stands for relative humidity.

977 **FIGURE 1**
978
979



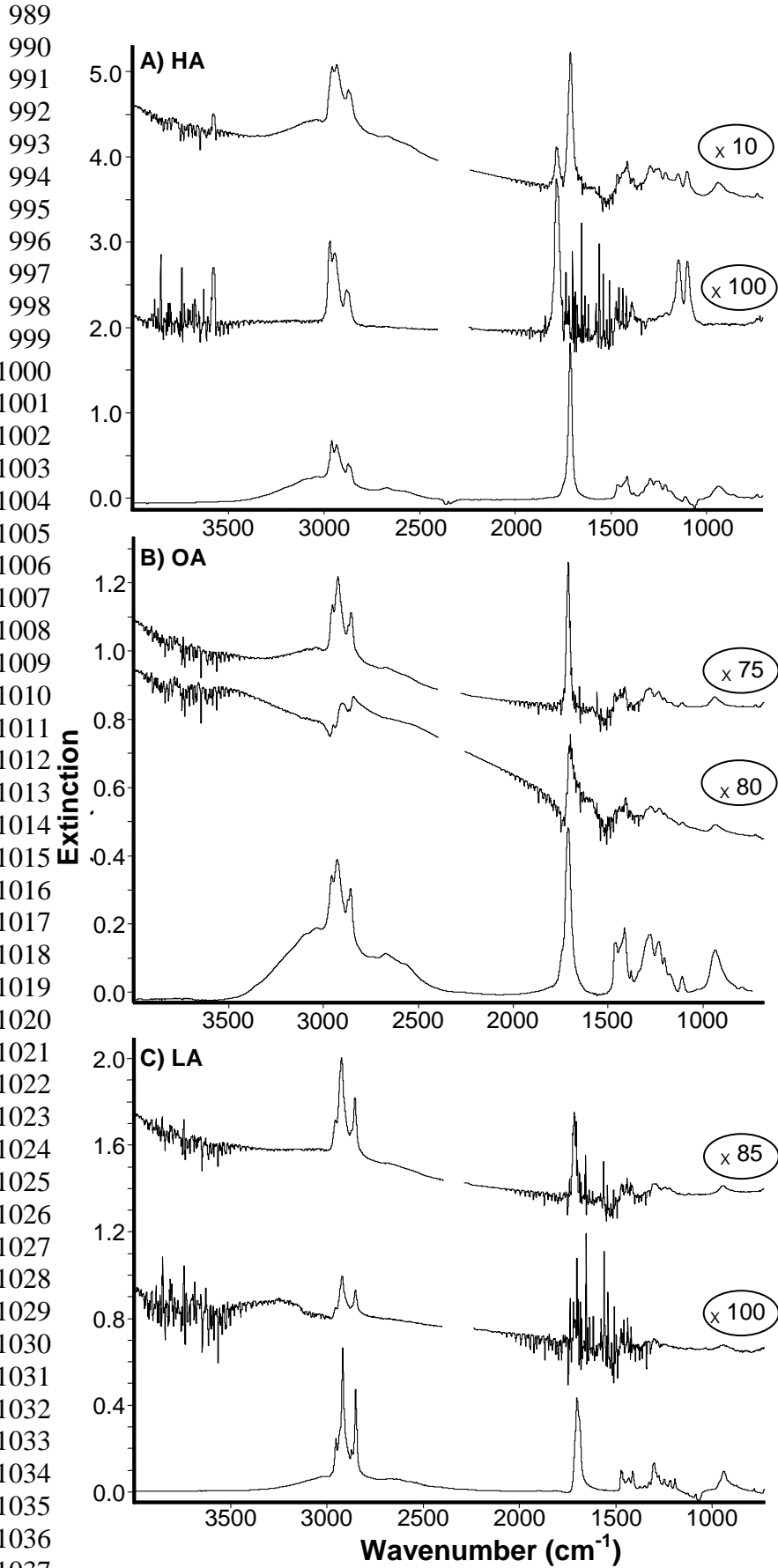
980
981

982 **FIGURE 2**
983
984

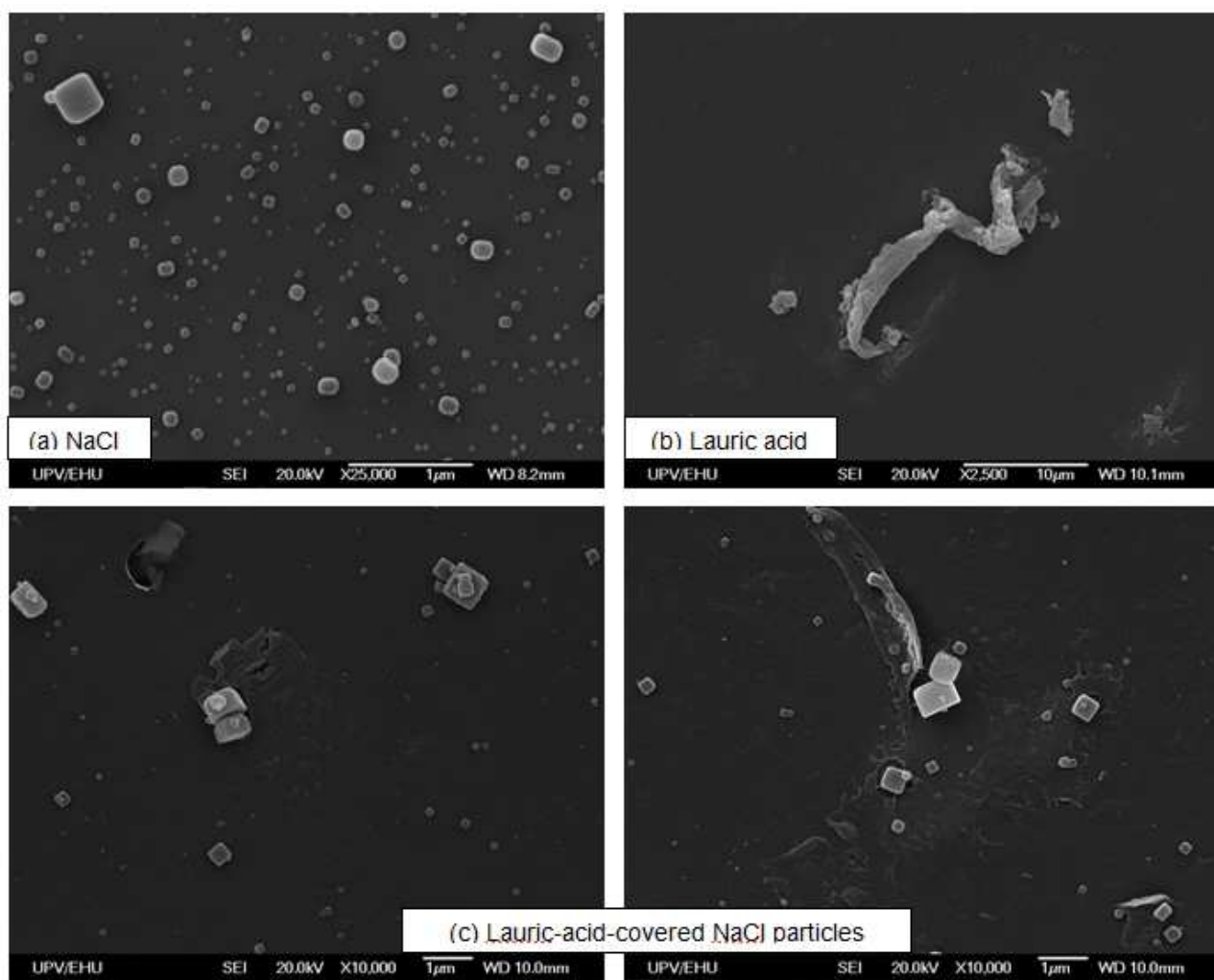


985
986
987

988 **FIGURE 3**

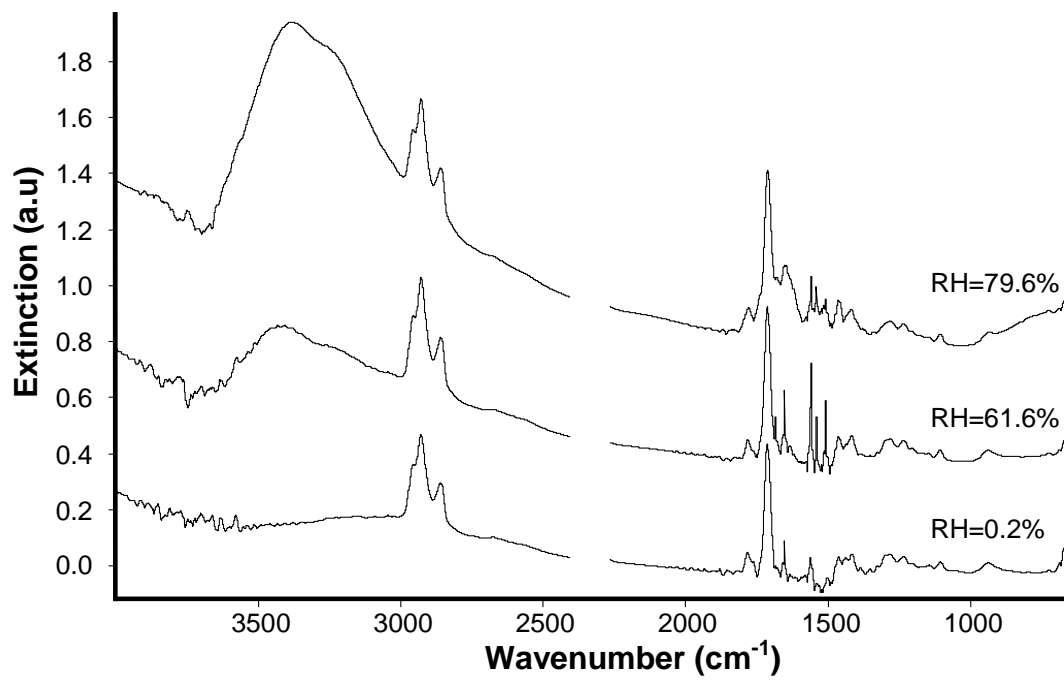


1039 **FIGURE 4**
1040
1041

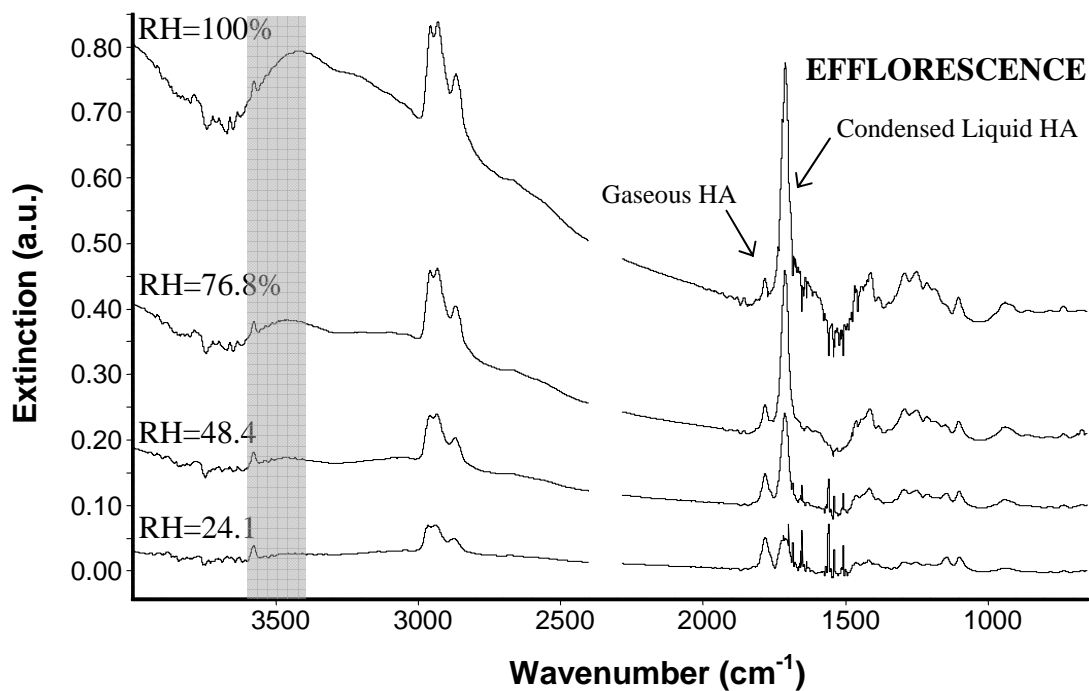
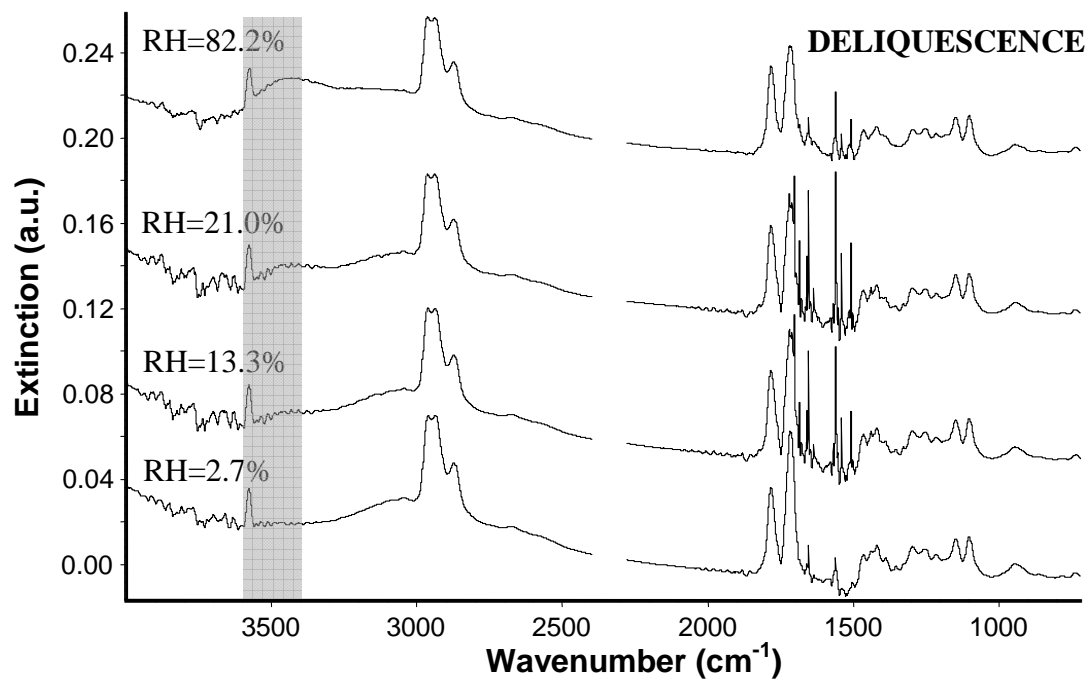


1042
1043

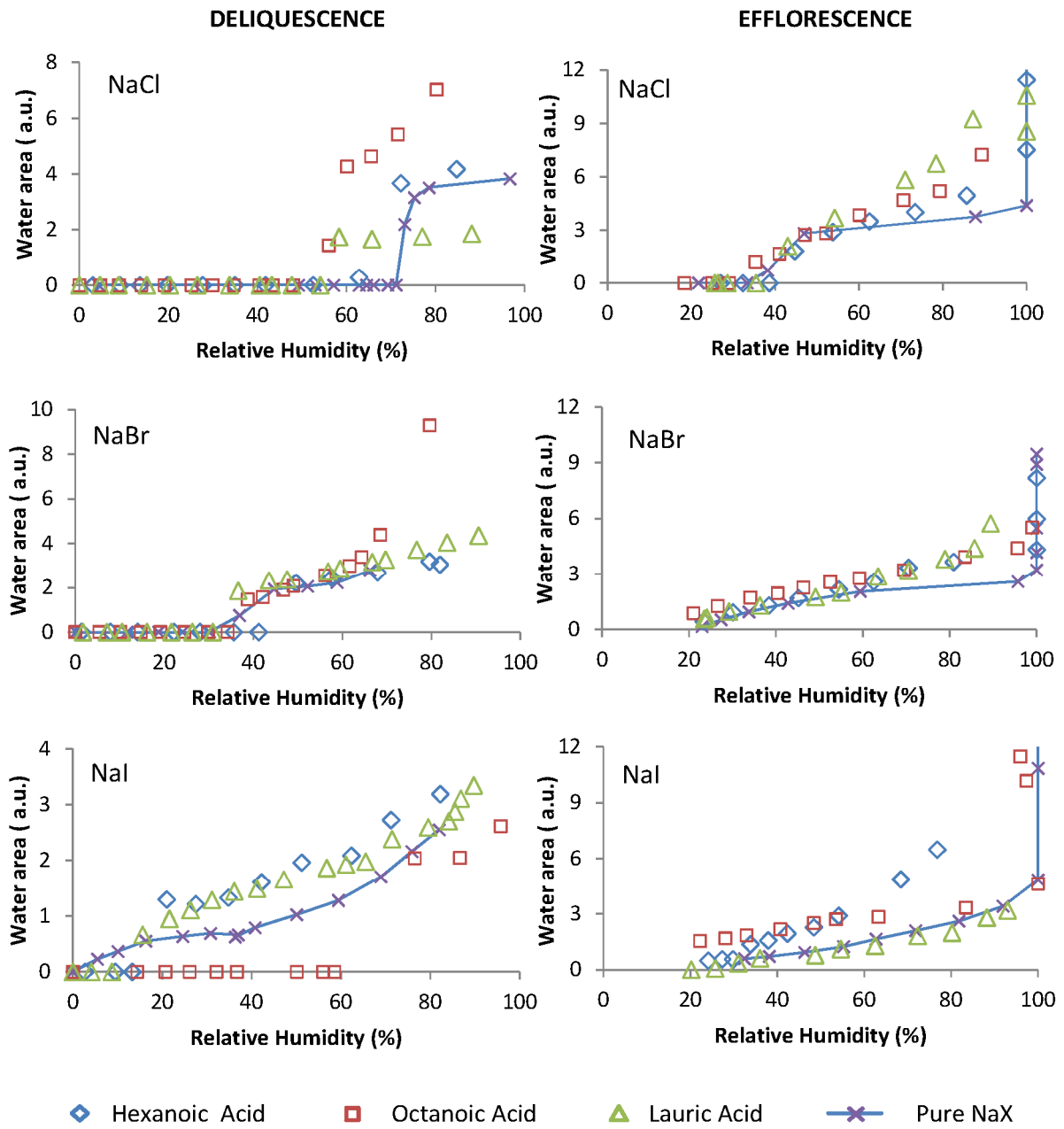
1044 **FIGURE 5**



1066 **FIGURE 6**

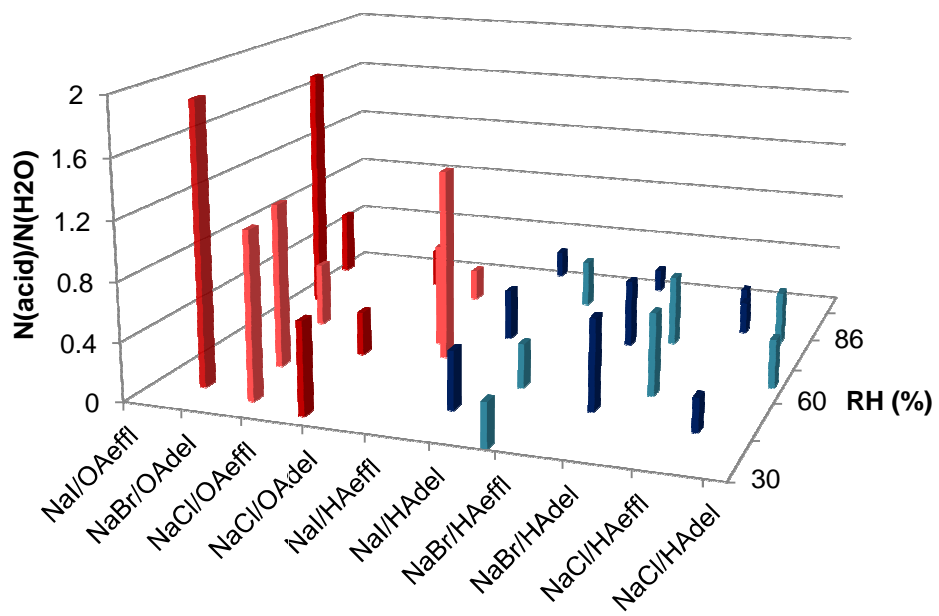


1111 **FIGURE 7**
 1112



1113
 1114

1115 **FIGURE 8**
1116

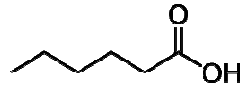
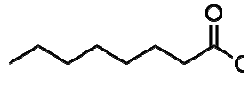
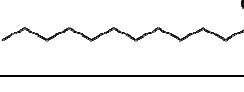


1117
1118

1119
1120
1121
1122

TABLE 1

Physical properties of the studied carboxylic acids

Name	#C	Structural Formula	Melting Point (K) ^a	Boiling Point (K) ^a	Vapour pressure (mm Hg, 25°C) ^b
Hexanoic Acid	6		269.7	477.±4	0.2
Octanoic Acid	8		289.3±0.7	510. ±4	3.71×10 ⁻³
Lauric Acid	12		317±2	571.	1.6×10 ⁻⁵

1123
1124
1125
1126
1127
1128
1129
1130
1131
1132

a: NIST Chemistry WebBook

b: PubChem Compound, NCBI (National Centre for Biotechnology Information)

#C Number of Carbon Atoms

1133 **TABLE 2**

1134

1135 Wavenumbers of the C=O stretching band in various conditions for HA, OA and LA. Units in cm^{-1}

1136

	Hexanoic acid (HA)		Octanoic acid (OA)		Lauric acid (LA)	
	band maximum	FWHM	band maximum	FWHM	band maximum	FWHM
gas ^a	1780	26	1780	62	1790	30
bulk	1710	20	1713	26	1700	29
homog. nucl.	1730	26	1700	46	1710	21
heter. NaCl ^b	1717	27-40 ^c	1707	19	1710	19
heter. NaBr ^b	1711-1720 ^c	27-37 ^c	1713	23	1708	26
heter. NaI ^b	1720	33	1713	36	1707	13

1137

1138

1139 ^a NIST Chemistry Webbook: <http://webbook.nist.gov/chemistry>1140 ^b Dry particles1141 ^c Depending on the amount of acid deposited onto the salt particles

1142